

**AEROSOL RETRIEVALS FROM INDIVIDUAL AVHRR CHANNELS:
II. QUALITY CONTROL, PROBABILITY DISTRIBUTION FUNCTIONS,
INFORMATION CONTENT, AND CONSISTENCY CHECKS OF RETRIEVALS**

Alexander Ignatov¹ and Larry Stowe²

*¹CIRA Visiting Scientist, NOAA/NESDIS, Office of Research and Applications,
Climate Research and Applications Division, Washington D.C. 20233, USA*

²NOAA/NESDIS, Office of Research and Applications,

Climate Research and Applications Division, Washington D.C. 20233, USA

Corresponding author's address: Dr. Alex Ignatov

phone (301)763-853 (ext. 190)

fax (301)763-8108

email: Alex.Ignatov@noaa.gov

Submitted for publication in the Section "Articles", Journal of the Atmospheric Sciences

16 December, 2000

Manuscript received: _____

26 June, 2001

Manuscript received: _____

Abstract

This second part of a two-part study evaluates retrievals of aerosol optical depths, τ_1 and τ_2 , in AVHRR channels 1 and 2 centered at $\lambda_1=0.63$ and $\lambda_2=0.83$ μm , and an effective Angstrom exponent, α , derived therefrom as $\alpha=-\ln(\tau_1/\tau_2)/\ln(\lambda_1/\lambda_2)$. The retrievals are made with the 6S radiative transfer model from four NOAA14/AVHRR datasets, collected between February 1998 - May 1999 in the latitudinal belt of 5-25°S. A series of quality control (QC) checks applied to the retrievals to identify outliers are described. These remove a total of ~1% of points, which presumably originate from channel mis-registration, residual cloud in AVHRR cloud screened pixels, and substantial deviations from the assumptions used in the retrieval model (e.g. bright coastal and high altitude inland waters). First, from examining histograms of the derived parameters it is found that τ and α are accurately fit by log-normal and normal probability distribution functions (PDF), respectively. Second, the scattergrams “ τ_1 vs τ_2 ” are analyzed to see if they form a coherent pattern. They do indeed converge at the origin, as expected, but frequently are outside of the expected domain in τ_1 - τ_2 space, defined by two straight lines corresponding to $\alpha=0$ and $\alpha=2$. This results in a low bias in α , which tends to fill in an interval of $\alpha \in [-1, 1]$ rather than $\alpha \in [0, 2]$. Third, scattergrams of “ α vs τ ” are used to empirically confirm a previously drawn theoretical conclusion that errors in α are inversely proportional to τ . More in depth quantitative analyses suggest that the AVHRR derived Angstrom exponent becomes progressively more meaningful when $\tau > 0.2$. Geographical trends are studied to demonstrate that the selected ocean area is reasonably uniform to justify application of consistency checks to reveal angular trends in the retrievals. These checks show that in most cases, the artifacts in the retrieved τ and α are statistically insignificant. On average, our analysis suggests that the retrieved τ_1 , τ_2 , and α show a high degree of self- and inter-consistency, with the exception of a troublesome May 1999 dataset. The most prominent problem noticed so far is the inconsistency between τ_1 and τ_2 , persistent from one dataset to another, which calls for fine tuning some (non-aerosol model related) elements of the retrieval algorithm. These adjustments will be discussed elsewhere.

1. Introduction

Our companion paper (Ignatov and Stowe 2001; hereafter IS01) described independent retrievals of aerosol optical depths (AOD) from spectrally wide channels 1 and 2 of the Advanced Very High Resolution Radiometer (AVHRR) onboard the NOAA polar orbiting satellites. The retrievals are subsequently scaled to the monochromatic wavelengths of $\lambda_1=0.63$ and $\lambda_2=0.83$ μm , which according to IS01, most closely represent the AVHRR central wavelengths onboard different NOAA satellites. These scaled τ_1 and τ_2 are finally reported, along with an effective Angstrom exponent, derived from them as

$$\alpha = -\frac{\ln \frac{\tau_1}{\tau_2}}{\ln \frac{\lambda_1}{\lambda_2}} = \Lambda \times \ln \frac{\tau_1}{\tau_2}; \quad \Lambda = -\frac{1}{\ln \frac{\lambda_1}{\lambda_2}} \quad (1)$$

Here, Λ is the spectral separation factor between the channels, $\Lambda \approx 3.63$.

Physical principles and premises of the retrieval algorithm are analyzed in detail by Ignatov and Stowe (2000). Its technical implementation with a new radiative transfer (RT) model, 6S (Vermote et al. 1997), was documented in great detail in IS01, which also described the four NOAA14/AVHRR datasets, used to quantify the effects of transition. Here, the same data, collected in the 5-25°S global latitudinal belt in Feb'98 (N=67,092 retrievals), Apr'98 (N=78,269), Jan'98 (N=101,081), and May'99 (N=108,286), are used to empirically evaluate the retrievals of τ and α . Performing analyses with data collected under such a wide variety of geometrical and calibration conditions allows one to acquire a long-term (15 months) perspective of the algorithm's performance, and thus a more realistic appreciation of their robustness. The first three datasets are largely inter-consistent with each other, whereas the May'99 dataset shows anomalous behavior, most likely due to a large proportion of its observations being taken at high solar zenith angles $\theta_s > 60^\circ$ (more than half; see analysis in section 7 by IS01).

In this study, the data have been additionally screened for outliers using a set of specially

implemented procedures. Mathematically, these are based on methods of identifying unexplained points far from the centers of the respective data clusters (available from the statistical literature (e.g. Ostle and Malone 1988; Bevington and Robinson 1992). Physically, they may result from significant “nonstatistical fluctuations” (term by Bevington and Robinson 1992) of the actual radiances and/or retrieval conditions from those assumed (due e.g. to radiometer malfunction, a significant departure from the retrieval model’s ocean surface/atmosphere properties, or a different kind of surface/land, or residual cloud in the cloud screened sensor’s field of view). These situations are unavoidable in real-world experimental data, especially in large datasets. With this outlier analysis, we have identified and excluded about 1% of aerosol optical depth retrievals in each dataset. The QC checks, introduced in sections 2 and 3, are shown to result in more robust and predictable statistics for the retrieved parameters, especially their extreme values - minima and maxima.

In section 2, the probability distribution functions (PDF) of all three aerosol parameters, τ_1 , τ_2 , and α , are analyzed. It is found that AODs are accurately represented by log-normal PDFs. This fact is in agreement with the recent analysis by O’Neill et al. (2000), who employed AOD data of various types of aerosols, measured by AERONET sun-photometers (Holben et al. 1998), to empirically demonstrate that the log-normal PDF is a better reference for reporting AOD statistics than the more customary normal PDF. Note that ocean bio-optical parameters often have PDFs close to log-normal (Campbell 1995), as do some of the atmosphere-optical parameters, e.g., aerosol backscatter (e.g. Tratt and Menzies 1994, and references therein), the liquid water path (Cahalan et al. 1995), and aerosol/cloud optical depth (King et al. 1980; Barker et al. 1996) (in the latter paper, a gamma distribution is used, which is close to log-normal, for a specific combination of parameters).

For the Angstrom exponent, a normal PDF was found to provide a reasonable fit to the data. The normality of the Angstrom exponent’s PDF was shown to be a direct consequence of the log-normality of the AOD PDFs. These fundamental results are important for many aerosol optics related applications,

as the vast majority of statistical methods and estimates imply, directly or indirectly, gaussian distributions of the data. An example of such an application is e.g. the space-time averaging of aerosol data (from either sun-photometer or satellite), and appropriate reporting of their statistics. Another example is validation of satellite aerosol retrievals through regression analyses against ground-based measurements. In the present study, the log-normal PDF is specifically used to put error bars on different statistical estimates, which gives yet another example of the practical use of this fundamental PDF result.

In section 3, the scattergrams of “ τ_1 vs τ_2 ” are analyzed in two different ways. The first analysis has to do with the quality control of retrievals, paving the way for one of the QC checks (referred to as QC1). Aimed specifically at identifying and removing those outliers (~0.5-0.8% of observations) which show up in the anomalous spectral behavior of τ , QC1 is based on a special cluster analysis of the “ τ_1 vs τ_2 ” regression residual. An interesting by-product from this part of the analysis is an estimate of two statistical parameters: an unresolved combination of rms errors in the retrieved τ_1 and τ_2 , $(\sigma_{1n}^2 + \sigma_{2n}^2)^{1/2} \sim 1 \times 10^{-2}$ (subscript “n” stands for “noise”), and the “natural” (noise-free) variability of the Angstrom exponent within the datasets, $\sigma_{no} \sim 0.24 \pm 0.02$ (represented with subscript “o”). The second analysis is related to checking the retrievals in the two channels for their inter-consistency, after the outliers have been removed. In particular, the scattergram is found to converge at the origin, as expected, but is shifted with respect to its expected domain, defined by two straight lines corresponding to $\alpha=0$ and $\alpha=2$. This results in a negative bias in α , which tends to fall in an interval of [-1,1] rather than the expected interval of [0,2].

Angstrom (1964) warned that the error in α derived from sun-photometers “reaches appreciable amounts first at low turbidity values”. Ignatov et al. (1998) have shown theoretically that errors in satellite derived α are inversely proportional to τ . Ignatov and Stowe (2000) found this theoretical prediction to be in good qualitative agreement with TRMM/VIRS aerosol retrievals. In section 4, errors in α are further structured into systematic trend, $\langle \alpha_{\epsilon} \rangle / \tau_1$ (hereafter, subscript “ ϵ ” refers to “error”), and

random error, σ_{ae}/τ_1 (brackets “ $\langle \rangle$ ” refer to “average”). Quantitative analysis of the scattergrams of “ α vs τ ” shows that the systematic trend component is negligible in many cases ($\langle \alpha_e \rangle \sim 0$), but noise is not: $\sigma_{ae} \sim 0.042 \pm 0.02$. The root-mean-squared “natural” (noise-free) variability in α is also estimated, and found to be $\sigma_{ao} \sim 0.22 \pm 0.02$, in agreement with estimates of section 2. Combining these, the cross-over point in AOD at which the “signal-to-noise” ratio in the Angstrom exponent, defined as $\eta = (\sigma_{ao}/\sigma_{ae}) \times \tau_1$, becomes 1 is found to be at $\tau_1 \sim 0.18 \pm 0.02$. This implies that the derived Angstrom exponent becomes progressively more meaningful as τ_1 exceeds ~ 0.2 , and progressively less meaningful as τ_1 diminishes from 0.2. This further emphasizes the point stated elsewhere (Ignatov et al. 1998; Ignatov and Stowe 2000) that the high noise in a size parameter at low τ is an inherent aerosol retrieval problem with any satellite radiometer, and with any size parameter (e.g., α) being derived with any aerosol retrieval algorithm. Despite some differences in robustness and accuracy, which depend on the choice of retrieval algorithm and retrieved size parameter and space/time averaging of the retrievals, the major restrictions to accuracy are being imposed by two mechanisms: the errors in different channels (due to radiometric and retrieval model uncertainties), and their spectral separation, which defines the amplification effect of these errors in the retrieved size parameter.

In section 5, angular trends in the retrievals are analyzed. Minimum and mean (along with its standard error) are plotted in each angular bin against sun, view, single scattering, and glint (angular distance away from specular reflection) angles. Note that statistics of AODs are calculated geometrically, due to the log-normality of their PDFs, whereas the Angstrom exponent statistics are calculated arithmetically. Within the uncertainty limits estimated from the observed PDF statistics, in the vast majority of cases there are no statistically significant angular trends in the mean values of τ_1 , τ_2 , and α . However, the minima show trends with almost every single angle. Possible reasons for these, and ways to alleviate them, are discussed.

In section 6, geographical trends in the retrievals are illustrated, and found to be small enough to

warrant the use of the angular tests of section 5. Also, the observed residual non-uniformities are consistent with intuitive expectations of the distributions of these parameters.

The major points of the study are summarized in the Conclusion section. In practical perspective, the two independent channel retrieval algorithm implemented with the 6S radiative transfer model was found to perform predictably and understandably, the retrievals revealing a high degree of self- and inter-consistency. However, some adjustments to the algorithm are needed. These will be considered in future papers.

2. Probability Distribution Functions of Aerosol Optical Depth and the Angstrom Exponent

a. Quality Control (QC) Tests

Only data that pass a series of specially formulated quality control (QC) tests, are used in the PDF analyses of this section. In applying QCs, a cumulative logic is used, i.e., QC2 is applied to the output of QC1; QC3 - to the output of QC2, and so on. A statistical summary of the results of application of different QCs is presented in Table 1.

First, data have been screened using a spectral test, QC1, described in detail in section 3. QC1 is applied before any other test, because it removes the vast majority of outliers resulting from significant violation of the retrieval assumptions. Technically, those anomalous retrievals are identified by their inconsistent appearance in the scatterplots of “ τ_1 vs τ_2 ”.

Second, points with negative AODs ($\tau_1, \tau_2 \leq 0$) were excluded (QC2-3). Those may result from a satellite sensor data error, or from a violation of the assumptions made in the retrieval algorithm (overestimated Rayleigh and/or oceanic contribution, etc; examples are discussed in section 3). The negative retrievals are physically unrealistic, but are useful to diagnose algorithm performance and/or data quality, and therefore are permitted in the original data. They are removed here to eliminate data points for which a logarithm cannot be calculated (needed for log-normal analyses below). They will be

allowed when analyzing minimum τ in sections 5&6. Table 1 shows that only two of the four datasets originally contained negative retrievals: Apr'98 (6 points with $\tau_1 \leq 0$; no negative retrievals in channel 2) and May'99 (115 points with $\tau_1 \leq 0$; and 7 points with $\tau_2 \leq 0$). Of these, only 30 points in May'99 with $\tau_1 \leq 0$ failed to be removed by QC1.

The third set of QCs (4&5) check τ_1 and τ_2 , separately, for outliers (i.e., atypical values). Several such tests are available from the statistical literature. The simplest one, the so called 4σ -test, has been selected. According to Ostle and Malone (1988) and Bevington and Robinson (1992), the probability of finding observations beyond a $\pm 4\sigma$ departure from an ensemble mean is negligible. It needs to be emphasized that the data being tested do not need to be distributed normally. The only requirements are that their PDF be mound-shaped, and reasonably symmetric. It will be shown that space/time ensembles of τ in both channels are closely described by log-normal distributions, which are strongly asymmetric about the peak. As a consequence, their logarithms are distributed more symmetrically (almost normally), and therefore are better suited to the 4σ -test. Another advantage of removing outliers in log-space is that the respective probabilities of occurrence can be estimated numerically. According to (Bevington and Robinson 1992), the probability of finding observations beyond a $+4\sigma$ departure for a normally distributed value ($> \log \tau_{gi} + 4 \log \mu_i$; QC4-5) is $\sim 3 \times 10^{-5}$, and the same probability exists for finding them beyond a -4σ departure ($< \log \tau_{gi} - 4 \log \mu_i$; QC6-7) (see next section for definitions of τ_g and μ). Therefore for $N \sim 10^5$ measurements in each ensemble, only about 3 data points are expected to be identified above and below the 4σ interval.

Table 1 shows that from 5 to 53 points are identified in channel 1 (QC4), and 1-4 *additional* points in channel 2 (QC5) (note that QC5 is applied to the output of QC4). Observations with $\log \tau > \log \tau_{gi} + 4 \log \mu_i$ are most probably due to residual cloud contamination in the data, mis-identified by the cloud-screening algorithm as clear. The small percentage of large AODs removed by QC4-5, is indicative of the very high quality of cloud screening in the AVHRR data (McClain et al. 1989). With

little doubt, cloud screening is of comparable (if not greater) importance for accurate aerosol remote sensing than the aerosol retrieval algorithm itself. Note also that the QC4-5 tests do a reasonable job of stabilizing $\tau_{1\max}$ and $\tau_{2\max}$ in the datasets (bottom two rows in Table 1), lowering them from 1.0-1.4 in channel 1, and 0.7-1.5 in channel 2, down to ~ 0.5 - 0.6 in both channels in all four datasets.

Many more data points are excluded at the low- τ end of the ensemble by QC6-7. The reason is that the *absolute* τ -errors (resulting from data errors and/or violations of model parameters, prescribed in the retrieval algorithm) translate into appreciably larger *relative* (per-cent) errors at small τ , thus resulting in larger *absolute* errors in $\log \tau$. As a result, many low- τ points fall below the critical 4σ interval: from 37 to 354 in channel 1, and *additionally* (again, recall that QC7 is applied to the result of QC6) from 31 to 178 in channel 2. The number of low-aerosol points excluded in both channels with QC6 and 7, respectively, shows an increasing trend in time, which may indicate an overall declining trend in both τ_1 and τ_2 . This trend is also clearly seen in $\tau_{1\min}$ and $\tau_{2\min}$ after screening (from ~ 0.04 in Feb'98 down to ~ 0.02 in May'99 in Table 1), which also become more uniform across the datasets. This feature will be discussed below in more detail.

Note that QC6-7 implies automatic removal of negative retrievals, so there may be no need for QC2-3. However, QC2-3 were introduced to specifically highlight the frequency of occurrence of negative retrievals in the data, which is, by itself, an independent indicator of the data/algorithm quality.

All seven tests together remove from 0.8-1.3% of the data. It should be particularly emphasized that more stable min/max statistics of AODs occur in both channels as a result of screening. In section 4, it will also be shown that the QCs have a favorable impact on Angstrom exponent retrievals.

b. PDF of Aerosol Optical Depths

Figs.1&2 show histograms of the screened AODs in channels 1 and 2, respectively, for the four datasets. Left panels show histograms of τ , and right panels - histograms of their decimal logarithms, \log

τ . (Hereafter, “log” refers to decimal logarithm, \log_{10} , while “ln” represents natural logarithm, \log_e).

In addition, their fit with a normal (in “log τ ” - space) and log-normal (in “ τ ” - space) PDF is shown (solid curves) according to the following two formulae (O’Neill et al. 2000):

$$P(\log \tau_i) = \frac{1}{\sqrt{2\pi} \log \mu_i} \times \exp \left[-\frac{\log^2 \frac{\tau_i}{\tau_{gi}}}{2 \log^2 \mu_i} \right]; \quad P(\tau_i) = \frac{1}{\tau_i} \times \frac{1}{\ln 10} \times P(\log \tau_i) \quad (2)$$

Here, τ_{gi} and μ_i are the geometric mean and standard deviation of τ_i in channel i ($=1,2$), defined as

$$\log \tau_{gi} = \langle \log \tau_i \rangle; \quad \log \mu_i = \sqrt{\langle (\log \tau_i - \langle \log \tau_i \rangle)^2 \rangle} \quad (3)$$

Similarly to O’Neill et al. (2000), these fits are not in the root-mean-squared sense (based on minimum residuals) but rather in the sense of determining how well the respective PDFs, given the same mean, standard deviation, and number of measurements as the data, fit the histogram. Visual inspection of histograms and their log-normal fits in Figs.1&2 suggests that in all cases, the respective histograms are close to log-normal. The quality of the fit is better in channel 1 than in channel 2, and for the first three datasets (Feb’98-Jan’99) than for the fourth (May’99). As discussed below, both the retrieval algorithm and the input satellite reflectances (calibration) probably need adjustment. Before these are made, any quantitative analysis of the goodness of the fit may be misleading, and therefore is not attempted herein.

The τ - satellite product being analyzed is a combination of a physical signal (AOD itself), with errors due to retrieval uncertainties (biases and scatter from deviations of the observed surface and atmospheric parameters from those prescribed in the model) and instrumental errors (calibration, noise, channel mis-registration, etc.) super-imposed on it. Therefore, even assuming that the physical signal is perfectly log-normal, certain deviations of the histograms from this ideal pattern are expected due to these errors.

From this perspective, two features of Figs.1&2 are worth noting. First, they suggest that the retrievals in AVHRR channel 1 are, overall, more accurate than in channel 2. They also imply that the retrieval errors increase towards the end of the 16-month observation period. Furthermore, if one assumes that additive (non-multiplicative) errors in the retrieved τ were about the same over the full range of τ (an assumption, not absolutely unrealistic), it would be the low-end of this range that would be subject to the largest relative (per-cent) errors, which would result in the largest absolute errors in $\log \tau$ (cf. with section 2a). Therefore, one could expect the largest distortions to be observed at low τ . Indeed, this feature seems to be observed in Figs.1&2(b), particularly in the May'99 dataset. This asymmetry may suggest that a better fit can be achieved from a truncated histogram, to minimize the effect of non-aerosol related noise at low τ , or through fitting the real histogram with a superposition of e.g. log-normal (“physical signal”) and normal (“noise”) PDFs. These more sophisticated analyses are not attempted, in anticipation of future improvements to the retrievals.

Arithmetic mean, τ_a , is often used in the remote sensing community as a measure of the total amount of aerosol over a certain ensemble of points (e.g. Husar et al. 1997; Wagener et al. 1997; Mishchenko et al. 1999; Higurashi and Nakajima 1999). According to O’Neill et al. (2000) and the present analyses, the use of *geometric* mean, τ_g , is a better characterization of AOD statistics, which allows for a more accurate reconstruction of the PDF, and is therefore better justified.

Table 2 lists geometrical means and standard deviations (τ_{gi} and μ_i , top), along with the regular arithmetic counterparts (τ_{ai} and $\sigma\tau_i$, bottom), for all four datasets. The values of τ_{ai} and τ_{gi} change coherently, with τ_{ai} being about 0.010 ± 0.002 higher than its respective geometric counterpart, τ_{gi} , in both channels. This suggests that either one or the other statistic can be used when mean values from different sources are compared (e.g. in validation of satellite retrievals against sun-photometers), as long as the same statistics are used consistently with both data sources.

In all four cases, on average, τ_1 exceeds τ_2 , as is expected from other independent observations

(e.g. Kaufman 1993; Tanre et al. 1997; Holben et al. 1998). This tendency holds in both the arithmetic and geometric sense (Quantitative analysis later in the paper shows, however, that the observed spectral difference is smaller than expected).

AODs in both channels show a clear declining trend with time (in both geometric and arithmetic senses), persistent from one dataset to the next. From Feb'98 through May'99, τ_1 declines by ~ 0.03 , and τ_2 by ~ 0.04 , which is about 25-35% of τ themselves. Some of this trend is undoubtedly a result of the change in calibration drift correction coefficients implemented in December 1998 (discussed in IS01, with numerical estimates of the effect). Also, some unpublished analysis of the monthly mean tropical time series of AOD from the AVHRR Pathfinder Atmosphere dataset (Stowe et al. 2001), shows that month to month changes within a year may be of comparable magnitude to the changes observed in Table 2 and may exhibit several maxima and minima within a given year. Also, latitudinal coverage in the 5-25°S region is changing with time, as illustrated in Fig.4 of IS01, such that any latitudinal gradients in AOD will be sampled differently, and may cause artificial changes in the 5-25°S mean values (either geometric or arithmetic).

Other possible causes of the declining trend in AOD could be related to the retrieval algorithm itself (e.g., due to a systematic change in scattering, illumination, or reflection geometry from one dataset to the other). Below, these hypotheses are explored with the data.

Errors in the aerosol microphysical model used in the retrieval algorithm have a multiplicative effect on τ (see e.g. Ignatov and Stowe 2000). Their effects on τ_{\min} are negligible, but not so on the mean τ , which is influenced in proportion to τ itself. Therefore these aerosol related errors may cause the observed downward trend of the mean (but not minimum) with time. These errors are introduced primarily through changes in the scattering geometry. The two datasets for Feb'98 and Jan'99 have similar scattering geometries (modal scattering angle $\chi \sim 170^\circ$), and therefore similar values of the scattering phase functions are used in both retrievals. However, these datasets show big differences in

AODs, thus denying the hypothesis that these deficiencies result from aerosol model errors.

If one assumes that it is the illumination geometry which exposes the aerosol model related errors, than the mean τ for Apr'98 and Jan'99 datasets should agree. They have similar sun illumination geometries (modal sun angle $\theta_{sm} \sim 50^\circ$), however, they also show big differences in the retrievals. On the other hand, the Feb'98 and Apr'98 datasets show negligible changes in AODs, whereas their sun-scattering geometries differ significantly (modal angles $\theta_{sm} \sim 37^\circ$, $\chi_m \sim 170^\circ$ in Feb'98; and $\theta_{sm} \sim 50^\circ$, $\chi_m \sim 150^\circ$ in Apr'98). It is therefore concluded that the observed trends are unlikely to be related to multiplicative errors in the data ($\sim 25\text{-}30\%$), which rejects the hypothesis that errors in the aerosol part of the retrieval algorithm are causing the trend.

From the above analyses, the errors causing the trend are most probably additive. This type of error is most easily seen in τ_{1min} and τ_{2min} (last rows in Table 1, and detailed analysis of section 5). These are substantially less related to aerosol model than are the average AODs, and are mostly defined by the surface reflectance model, the Rayleigh optical depth used in the retrieval model, and the calibration of the satellite sensor. If this downward trend is related to the surface reflectance model, then trends in the retrievals must be due to systematic changes in illumination-viewing geometry. However, it was shown above that there is no direct correlation between geometry and the trends.

We therefore conclude that systematic trends in the calibration of the two AVHRR channels are most likely to be the cause. According to our estimates, a drop of $\sim 6\text{-}8\%$ in the calibration slope over the period of Feb'98-May'99 would explain the observed trend in τ . This is in fact what occurred in December 1998 when calibration drift coefficients were changed (cf. Eqs.(10-12), IS01). The largely coherent decline in the two channels may be related to the methods employed in the vicarious calibration procedure, which separates the systematic change of illumination geometry from sensor degradation over a bright desert target (Rao and Chen 1996).

b. PDFs of the Angstrom Exponent

Fig.3a shows histograms of the Angstrom exponent, α , for retrievals which passed all seven QC tests, described in section 2a, whereas Fig.3b shows a sub-sample of those for which $\tau_1 \& \tau_2 \geq 0.1$ (the meaning of this second panel is explained below), along with their fit with a normal PDF (defined in the same sense as above for τ):

$$P(\alpha) = \frac{1}{\sqrt{2\pi}\sigma_\alpha} \times \exp\left[-\frac{(\alpha - \alpha_m)^2}{2\sigma_\alpha^2}\right] \quad (4)$$

where α_m and σ_α are ensemble arithmetic mean and standard deviation of the Angstrom exponent. To demonstrate that a normal PDF is appropriate, Eq.(1) can be re-written as

$$\alpha = \frac{\Lambda}{\log e} \times (\log \tau_1 - \log \tau_2)$$

Being a linear combination of two normally distributed values, $\log \tau_1$ and $\log \tau_2$, α is also expected to be distributed normally (e.g. Ostle and Malone 1988).

The shape of the histogram of α in Fig.3a is, indeed, close to gaussian. In all cases, the fit matches the mode of the histogram, α_m , but overestimates the width of the distribution, σ_α , which may be due to errors in the retrieved α , as it was with τ . It will be shown in section 4 that the measured signal is a combination of a physical signal (i.e., “true” wavelength dependence of τ at two wavelengths), with an error that increases in inverse proportion to τ . This has already been discussed in section 2, that larger *absolute* errors in $\log \tau$ occur at lower τ . According to the above equation, errors in τ are amplified when combining τ_1 and τ_2 into the Angstrom exponent, which should result in widening of its histogram. To test this hypothesis, in the right panel of Fig.3 are plotted histograms of α after excluding small τ values (i.e., only $\tau_1 \& \tau_2 > 0.1$ are used). Overall, they and their PDF fits become much closer to normal, although the fit continues to show a somewhat flatter shape as compared to the more peaked data in three of the

four datasets.

Quantitative information on the two fit parameters, α_m and σ_a , for the two cases presented in Fig.3 (all data passed QC1-7, and a sub-sample of those with $\tau_1 \& \tau_2 > 0.1$), is given in the bottom portion of Table 2. As Fig.3 suggests, the sample standard deviation of the Angstrom exponents (σ_a) is more sensitive to the restrictions imposed on τ , than the sample mean (α_m). There is no clear time trend in the derived Angstrom exponent as there is in τ . The fluctuations are within a few hundredths of 0.1 in the first three datasets, and of ~ 0.4 in the May'99 dataset.

It is concluded from these analyses that the PDF of the true Angstrom exponent is close to gaussian. Any deviation of the observed empirical histogram from this function most probably results from non-aerosol related errors in the retrievals, due to input data quality and deviations of actual retrieval conditions from those assumed in the retrieval model. It is also concluded that despite noticeable trends in τ_1 and τ_2 , these trends appear to be largely coherent in the channels, and cancel out when taking their ratio in calculating the Angstrom exponent, except for the May'99 dataset.

3. Scattergrams “ τ_1 vs τ_2 ”

If τ_1 and τ_2 are error-free, then scattergrams of “ τ_1 vs τ_2 ” shown in Figs.4-7(a1) (one figure for each of the four datasets), would form a compact spectrally-coherent cluster, located in a triangular sector of the two-dimensional “ τ_1 - τ_2 ” space. In reality, the retrievals are prone to different errors, which result in two types of distortion to this expected pattern: 1) outliers, falling outside of this cluster, and 2) displacement of the actual cluster from its expected domain. In the two sub-sections below, outliers are identified and then removed by using a specially developed statistical procedure, based on the expected spectral coherence of the retrievals, and then, the location of the cluster with respect to its expected domain is examined.

a. Spectral QC Test of the Retrievals (QC1) to Remove Outliers

Eq.(1) suggests that if τ_1 and τ_2 are error-free, i.e. $\tau_1 = \tau_1^t$, $\tau_2 = \tau_2^t$ (the superscript “t” here stands for “true”), then their values, according to Eq.(1), would be linearly related as¹

$$\tau_1^t = a^t \times \tau_2^t; \quad \text{where } a^t = \exp\left(\frac{\alpha_o}{\Lambda}\right) \quad (5)$$

where α_o represents the “true” (error-free) Angstrom exponent.

The retrieved τ_1 and τ_2 , however, are not error-free. They are subject to channel (*i*)- and retrieval-point-specific multiplicative, ξ_i (e.g. due to error in aerosol phase function, molecular absorption, or calibration) and additive, ε_i (e.g. due to uncertain oceanic reflectance, Rayleigh scattering, or radiometric noise) errors (Ignatov and Stowe 2000), represented as

$$\tau_1 = \xi_1 \times \tau_1^t + \varepsilon_1 \quad \tau_2 = \xi_2 \times \tau_2^t + \varepsilon_2 \quad (6)$$

Combining Eqs.(5-6), the relationship between the two retrieved AODs is re-written as

$$\tau_1 = a \times \tau_2 + b; \quad a = a^t \times \frac{\xi_1}{\xi_2}; \quad b = \left(\varepsilon_1 - \varepsilon_2 \times a^t \times \frac{\xi_1}{\xi_2} \right) \quad (7)$$

Eqs.(5-7) are written for each individual retrieval point (AVHRR observation), and therefore, τ_1 and τ_2 are instantaneous retrievals, and all other parameters are retrieval-point specific.

Let us now consider the ensemble of observations presented in Figs.4-7(a1), and fit a linear regression line through the scattergram²:

¹In what follows, τ_2 is considered an independent, and τ_1 , a dependent variable. This is not critical to the analysis since the two variables can be switched, which will change the intermediate considerations, but not the final result.

²Analysis of section 2 suggests that, from a statistical point of view, the linear regression analysis would be more adequate to perform in a “ $\log \tau_1$ vs $\log \tau_2$ ” rather than “ τ_1 vs τ_2 ” space. However, transition to a log-space automatically requires excluding negative retrievals, before the outlier analysis is done, which eliminates these obvious retrieval errors from further diagnoses.

$$\hat{\tau}_1 = a_o \times \tau_2 + b_o; \quad \Delta \tau_1 = \hat{\tau}_1 - \tau_1; \quad \sigma_{\Delta \tau_1}^2 = \overline{(\hat{\tau}_1 - \tau_1)^2} \xrightarrow{a_o, b_o} \mathbf{min} \quad (8)$$

Figs.4-7(a1) suggest that the scattergrams tend to diverge as AOD increases, due to aerosol size related variability in the Angstrom exponent, consistent with Eq.(5) (cf. with Ignatov and Stowe 2000, and analysis in the next sub-section). This diverging pattern is somewhat more clearly seen in Fig.4-7(a4), which is a plot of the residual of the regression $\Delta \tau_1$ as a function of τ_2 . In addition, Figs.4-7(a2) show histograms of the regression residual, $\Delta \tau_1$, defined by Eq.(8), along with its gaussian fit, whose quality will be shown to improve after outlier removal³.

Given that the retrieval errors ξ_i and ε_i may vary from one retrieval point to another, as also may the Angstrom exponent (and therefore the a' parameter defined by Eq.(5)), the residual, $\Delta \tau_1$, and its variance, $\sigma_{\Delta \tau_1}^2$, for a given value of τ_2 , are described as

$$\Delta \tau_1 = \hat{\tau}_1 - \tau_1 = \Delta a \times \tau_2 + \Delta b; \quad \sigma_{\Delta \tau_1}^2 = \overline{(\hat{\tau}_1 - \tau_1)^2} = \sigma_a^2 \times \tau_2^2 + \sigma_b^2 \quad (9)$$

Here, $\Delta a = a_o - a$, $\Delta b = b_o - b$, where (a, a_o) and (b, b_o) are defined by Eqs.(7-8), and their respective variances are

$$\sigma_a^2 = \sigma^2 \left(a' \times \frac{\xi_1}{\xi_2} \right); \quad \sigma_b^2 = \sigma^2 (\varepsilon_1) + \sigma^2 \left(\varepsilon_2 \times a' \times \frac{\xi_1}{\xi_2} \right) \quad (10)$$

Eq.(10) can be simplified, for the convenience of further semi-quantitative estimates. In its first part (for σ_a^2), multiplicative errors are assumed minimal ($\xi_1 \sim \xi_2 \sim 1$, and therefore $\xi_1/\xi_2 \sim 1$), and the a' -term (defined by Eq.(5)) is assumed to be represented by a truncated Taylor series: $\exp(\alpha_o/\Lambda) \sim 1 + \alpha_o/\Lambda$. In the second

³The residual of regression, defined by Eq.(8), $\Delta \tau_1$, is composed of the variability in the Angstrom exponent (which was shown to be distributed normally), and additive retrieval errors. The latter result from many factors and therefore are also expected to be distributed normally according to the central limit theorem. The deviation of the histogram from the normal fit is thus expected to be mostly related to outliers. Note that the gaussian fit, in this particular case, is neither analyzed nor used in this paper in any quantitative manner but for illustration purposes only.

part of Eq.(10) (for σ_b^2), $a^t \sim 1$ is substituted⁴. This gives:

$$\sigma_a^2 \approx \frac{\sigma_{\alpha_0}^2}{\Lambda^2}; \quad \sigma_b^2 \approx \sigma_{1n}^2 + \sigma_{2n}^2 \quad (10a)$$

In Eq.(10a), $\sigma_{\alpha_0}^2$ [i.e. $\sigma^2(\alpha_0)$] is the natural (noise-free) variance of the Angstrom exponent, and σ_{1n}^2 and σ_{2n}^2 are variances of the τ -retrieval *additive* errors (“noise”). From Eq.(10a) one concludes that the σ_a -term is mostly related to the natural (noise-free) root-mean-squared variability in the Angstrom exponent within the dataset (σ_{α_0}), whereas the σ_b -term is mostly due to the combined root-mean-squared additive errors in the channels ($\sigma_{1n}^2 + \sigma_{2n}^2$)⁵.

The proportionality between $\sigma_{\Delta\tau_1}^2$ and τ_2^2 , suggested by Eq.(9) and shown in Figs.4-7(a3), serves as the basis from which to construct an iterative procedure to remove the outliers. First, the data points in Figs.4-7(a3) are fit with a linear regression line (suggested by Eq.(9), through the points, $\sigma_{\Delta\tau_1}^2$, estimated at binned values of τ_2^2), and the predicted $\sigma_{\Delta\tau_1}^2$ are used to remove points with $|\Delta\tau_1| \geq 4\sigma_{\Delta\tau_1}$ in Figs.4-7(a1). The reason for using the 4σ -threshold has already been discussed in section 2. After that, the regression coefficients (a_o, b_o) are re-evaluated, and the full analysis repeated until convergence is achieved, i.e. no points are found outside the $\pm 4\sigma_{\Delta\tau_1}$ interval.

Table 3 shows the number of iterations required to achieve convergence, along with the number of points excluded at each iteration step. Typically, 4-7 iterations are required, which exclude 0.5-0.8% of the measurements. The final result of this iterative procedure is presented in the right panels of Figs.4-7 (fully comparable in its structure with the left panels). All dependencies become more regular and less noisy, including a closer match to a gaussian fit in Figs.4-7(b2) and a better linear relationship “ $\sigma_{\Delta\tau_1}^2$ vs

⁴In fact, a^t varies from $a^t \sim 1$, when $\alpha_o \sim 0$, to $a^t \sim 1.74$, when $\alpha_o \sim 2$. For typical oceanic aerosols, $\alpha_o \sim 0.5$, and $a^t \sim 1.15$, which justifies the use of $a^t \sim 1$.

⁵Eq.(10) shows that both the $\sigma_{\alpha_0}^2$ - and σ_{2n}^2 -terms may need adjustment for a ratio of multiplicative errors in the channels. The latter term may additionally need adjustment for a non-zero Angstrom exponent. These adjustments are typically small, and therefore neglected here, for brevity and simplicity.

$\tau_2^{2''}$ in Figs.4-7(b3).

The outliers being removed by this iterative procedure may be due to either instrumental errors (e.g., noise in an individual channel, mis-registration between different channels, etc.), or to a violation of the physical retrieval model⁶. Below, a possible (but by no means exhaustive) explanation for some of them is given. Whatever the reason or explanation for a particular outlier, it must be excluded from aerosol related analyses as being indicative of either a problem with the radiometer data, or with the retrieval model at the particular retrieval point.

First, very few outliers fall below the -4σ boundary, but many more are above it (see e.g. Figs.4-5). Geographical location has shown that the low outliers typically belong to high-altitude lakes. Let us consider as an example the six points with $\tau_1 < 0$ collected on April 5, 1998 (these are not shown in Fig.5(a1), but they are included in Fig.5(a4) and noted in the second line of Table 1; note in Table 1 that for all six points, $\tau_2 > 0$). Those were located in Lake Titicaca in Peru ($\phi \approx 15-16^\circ\text{S}$, $\lambda \approx 69-70^\circ\text{W}$) at an altitude of 3,812 m. The operational retrieval algorithm considers all data more than ~ 15 km from a coast line to be suitable for retrieval. The reason for underestimating τ_1 is that the Rayleigh optical depth in channel 1, τ_1^R , is only ~ 0.035 over this high-altitude lake, i.e., it is ~ 0.025 lower than assumed for sea level in the retrieval algorithm. As a result, the measured reflectance in channel 1 is below what is expected for $\tau_1 = 0$ in the look-up-table, and a negative τ_1 is retrieved. Taking into account that an error in τ^R translates into an error in τ with an amplification of $\sim 5-6$ (for detail, see Ignatov and Stowe 2000), one can expect the error $\delta\tau_1 \sim -0.15$. In channel 2, τ_2^R is about 3 times less than in channel 1 (~ 0.02 at sea level), so $\delta\tau_2$ is three times less, i.e. ~ -0.05 . If AODs over the lake were about ~ 0.10 in both channels on April 5, 1998, then the estimated $\tau_1 \sim (0.10 - 0.15) \sim -0.05$, and $\tau_2 \sim (0.10 - 0.05) \sim +0.05$, which closely

⁶Analysis of Figs.4-7(b1) suggests that some points identified as outliers by the present procedure seem reasonable, as they have e.g. $0 < \alpha < 2$. Note that in many cases, this deceiving “goodness” of the excluded points is related to the overall displacement of the clusters from their expected domains, resulting from systematic errors in the retrievals. With this in mind, we choose to follow the advice from Bevington and Robinson (1988): “do not trust statistics in the tails of the distributions”.

correspond to those observed on that day. Table 1 suggests that these six points have been successfully identified by the spectral (QC1) test, due to the wavelength dependent effects of an inconsistency in surface altitude. This example originally motivated the development of the QC1 test, and was later extended to include QC2-7. Figs.4-7(a4) suggest that there are more points collected over high altitude lakes, which have both τ_1 & $\tau_2 > 0$ and would not be easily identified without multi-spectral measurements and tests like QC1.

Many more outliers tend to fall above the $+4\sigma$ boundary. Now, τ_1 appears to be *overestimated* relative to channel 2 (or τ_2 *underestimated* relative to channel 1), i.e., the measured value in channel 1 is higher than predicted from the measurement in channel 2, τ_2 . This class of outliers may originate from unscreened coastal waters in the retrievals (due perhaps to navigation errors). These tend to be much brighter than assumed in the retrieval model, and are much brighter in the channel 1 than in the channel 2 spectral region (e.g. Morel and Prieur 1977; Sathyendranath et al. 1989). This leads to a disproportionately larger overestimation of τ_1 than τ_2 , which allows QC1 to discriminate such cases.

It may not be the outliers (which are relatively easy to identify and remove from the retrievals) which are of the biggest concern, however. There are likely to be more retrievals which fail, for one reason or another, to meet the assumptions made in the retrieval algorithm, or are contaminated by measurement errors, but do not stand out as outliers. As Bevington and Robinson (1992) put it, “such (outlier) points may imply the existence of other contaminating points within the central probability region, masked by the large body of good points”. As a result, these points fail to be detected by the QC1 test (or any other test, for that matter), and will be mistakenly analyzed with valid aerosol observations. Thus, if a certain percentage of data is clearly identified as “bad” because they fall well outside the main body of “good” points, there are probably even more “good” points whose aerosol observation is distorted by errors of different types such that they are in the wrong subspace of the expected domain, or even fall outside of it. In this perspective, the number of identified and excluded “outliers” may be an

indicator of the overall quality of the data.

Figs.4-7 (b3) allow one interesting physical interpretation in terms of the formulated model. According to Eqs.(9-10a), the intercept of the straight line is, to a good approximation, $\sigma_b^2 \sim (\sigma_{n1}^2 + \sigma_{n2}^2)$, whereas the slope is $\sigma_a^2 \sim (\sigma_{ao}/\Lambda)^2$. For the first three datasets (Feb'98-Jan'99), the intercept is $\sigma_b^2 \sim 1 \times 10^{-4}$, and the slope is $\sigma_a^2 \sim (40 \pm 5) \times 10^{-4}$. It is impossible from the present analysis to separate contributions to σ_b^2 from each channel, σ_{n1} and σ_{n2} . Assuming them comparable, one obtains $\sigma_{n1} \sim \sigma_{n2} \sim 7 \times 10^{-3}$. The natural variability in the Angstrom exponent can be estimated from Eq.(10a) as $\sigma_{ao} \sim \sigma_a \times \Lambda$. Observing from Figs.4-7 (b3) that $\sigma_a \sim (6.5 \pm 0.5) \times 10^{-2}$, and substituting $\Lambda \sim 3.63$, one obtains that $\sigma_{ao} \sim 0.24 \pm 0.02$. This implies that the overall natural variability of the Angstrom exponent within each of the three datasets is $\sim \pm 3\sigma_{ao}$, i.e., within $\sim (1.45 \pm 0.10)$ units, which compares fairly well with the commonly used estimate of range of this parameter of ~ 2.0 . Statistics for the May'99 dataset differ from the first three datasets substantially, and are not given further consideration. More in depth analysis is needed to understand the overall anomalous nature of this dataset.

b. Scattergram of τ_1 vs τ_2 , after QC tests

Analysis of this sub-section concentrates on panel (b1) of Figs.4-7. These scattergrams after screening are expected to converge at the origin, where both optical depths are 0, and progressively diverge as τ increases, due to real changes in the Angstrom exponent as discussed in the previous sub-section and used in the development of QC1. This divergence should be bounded by two straight lines, defined by setting $\alpha=0$ and $\alpha=2$, i.e., all points should fall between the lines $(\tau_1 = \tau_2)$ and $(\tau_1 = 1.74\tau_2)$. This test, originally proposed for quality control of sun-photometer measurements by Korotaev et al. (1993), and later re-iterated by Ignatov and Stowe (2000), applied to VIRS retrievals, allows one to uncover *relative* (one channel with respect to the other) additive and multiplicative errors in τ .

Intercepts of the linear regression lines defined by Eq.(8), b_o , are small for all four datasets

($0 < b_o < 0.01$). This apparent agreement between the channels at low τ may, however, be deceiving. For example, if, as was shown in Table 2, both τ_1 and τ_2 decline over time by ~ 0.03 - 0.04 , these changes, (perhaps resulting from calibration drift correction errors) are, to a large extent, coherent in the two channels, thus masking the effect of these systematic trends in the two channels on their regression statistics.

The spread of the scattergram progressively increases towards higher τ , due to natural variability in the Angstrom exponent over the area (this feature has already been discussed in the previous subsection, and is used as the basis for QC1). The cluster, however, fails to fill in the entire area between the two diverging lines (corresponding to $\alpha=0$ and $\alpha=2$). Instead, the Angstrom exponent appears to be biased low, and tends to group around the lower expected boundary of the domain, $\alpha=0$. This indicates a systematic relative error introduced by the retrieval algorithm, in which either τ_1 is biased low, or τ_2 is biased high, or both. It is inconceivable that this bias is related to the aerosol microphysical model solely, which is expected to contribute no more than $\sim \pm 0.4$ to the uncertainty in α (IS01). Most probably, this bias is related to non-aerosol parameters. As a clear example, an overestimated water vapor absorption in channel 2 in the look-up-table (resulting in underestimated model radiances), would result in an overestimated τ_2 .

4. Scattergrams of “ α vs τ ”

Fig.8 shows scattergrams of α vs τ_1 for original data (left panel, a) and after screening with the QC1-7 tests (center panel, b), in four rows for each dataset. The three lines super-imposed are average trends in α (solid line), and the average plus-minus three standard deviations (broken lines), both calculated as explained below.

Comparison of the screened and original data continues to suggest that, in many cases, observations yielding spurious estimates of the Angstrom exponent have been successfully removed with

QC1-7. Remember that the QC tests have been developed and applied without any explicit use of the Angstrom exponent (albeit the QC1 test uses consistency between those channels used for the calculation of α). This further illustrates the value and effectiveness of the quality control procedures.

Ignatov et al. (1998) have shown, theoretically, that the error in the Angstrom exponent increases in inverse proportion to AOD. According to this theoretical result, the retrieved α for an arbitrary retrieval point can be represented as a superposition of a “physical” signal, α_p , and an error signal, α_e/τ , as:

$$\alpha = \alpha_p + \frac{\alpha_e}{\tau}; \quad \bar{\alpha} = \alpha_o + \frac{\alpha_{oe}}{\tau}; \quad \sigma_\alpha^2 = \sigma_{\alpha o}^2 + \sigma_{\alpha e}^2; \quad \sigma_{\alpha e}^2 = \frac{\sigma_{\alpha e}^2}{\tau^2} \quad (11)$$

A $1/\tau$ -type *trend* in the average would be indicative of a *systematic* error in α (i.e., if $\alpha_{oe} \neq 0$ in Eq.(11)), whereas a $1/\tau$ -type increase in *scatter*, symmetrical with respect to the average trend, would be indicative of a *random* error in the α retrievals (characterized in Eq.(11) by the $\sigma_{\alpha e}/\tau$ term).

Eq.(11) suggests that the variance of the Angstrom exponent, σ_α^2 , is proportional to $1/\tau^2$, with the proportionality coefficient being $\sigma_{\alpha e}^2$ [i.e. $\sigma^2(\alpha_e)$]. The respective correlation of these two variables is shown in Fig.8(c) for all four datasets. (One can use either τ_1 or τ_2 for τ in Eq.(11); here, we use τ_1). The overall quality of the linear fit to the data is quite satisfactory, although the relationship tends to level off at low $1/\tau_1^2$ (high τ).

The regression parameters of Fig.8(c) are largely consistent over the first three datasets, but the noticeably higher in the May’99 dataset. Similar to section 2, we do not include this latter anomalous dataset in the estimates below. The intercept is $\sigma_{\alpha o}^2 \sim 0.05 \pm 0.01$, so that $\sigma_{\alpha o} \sim 0.22 \pm 0.02$. This estimate is in remarkable consistency with the estimate in section 3, where this parameter was found to be $\sigma_{\alpha o} \sim 0.24 \pm 0.02$. The slope is $\sigma_{\alpha e}^2 \sim (18 \pm 2) \times 10^{-4}$, i.e., $\sigma_{\alpha e} \sim (4.2 \pm 0.2) \times 10^{-2}$.

The $\sigma_{\alpha e}$ - parameter can be estimated in a different way. From Eq.(1), $\alpha = \Lambda \times \ln(\tau_1/\tau_2)$. The measured τ_1 and τ_2 are subject to errors, as per Eq.(6). Assuming in Eq.(6) that errors in τ are purely

additive (i.e., $\xi_1 \& \xi_2 \approx 1$), and substituting Eq.(6) into a differentiated Eq.(1), one obtains for an error in α : $\delta\alpha = \Lambda \times \ln[(\tau_1^t + \varepsilon_1)/(\tau_2^t + \varepsilon_2)] - \Lambda \times \ln[\tau_1^t/\tau_2^t] \approx \Lambda \times [\varepsilon_1/\tau_1^t + \varepsilon_2/\tau_2^t]$. Assuming, for the sake of estimating the root-mean-squared error of α , that $\tau_1^t \sim \tau_2^t \sim \tau_1$, one obtains $\sigma_{an}^2 \sim (\Lambda/\tau_1)^2 \times (\sigma_{n1}^2 + \sigma_{n2}^2) \equiv (\sigma_{ae}^2/\tau^2)$, where $(\sigma_{n1}^2 + \sigma_{n2}^2) \sim 10^{-4}$ from section 3a. Substituting, one obtains: $\sigma_{ae} \sim \Lambda \times (\sigma_{n1}^2 + \sigma_{n2}^2)^{1/2} \sim 3.6 \times 10^{-2}$, in good quantitative agreement with the direct estimate above.

The above estimates of “physical signal” and “noise” in the Angstrom exponent allow one to define the “signal-to-noise” ratio from Eq.(11) as $\eta = \sigma_{ao}/\sigma_{an} = (\sigma_{ao}/\sigma_{ae}) \times \tau_1$. (Here, root-mean-squared deviations of the “physical signal” and “noise” are substituted for their measure, i.e., are used as their norm). The linear increase of η with τ_1 has clear physical meaning, and in particular, it suggests a “cross-over” point, τ_{1c} , to be defined, at which $\eta=1$. Numerical estimates show that $\tau_{1c} \sim (0.18 \pm 0.02)$. As τ_1 decreases from τ_{1c} , the measured signal is progressively more composed of “noise” (resulting from radiometric error, and fluctuations of the prescribed non-aerosol model parameters from those being observed). As τ_1 increases beyond τ_{1c} , the aerosol contribution to the estimated α increases above the noise, which is still present. For example, if $\tau_1 \sim 0.4$ (i.e. $\eta \sim 2$), about 2/3 of the measured α comes from the aerosol signal itself, while the remaining 1/3 is noise. Implications of this “information content” approach on the AVHRR-derived Angstrom exponent are discussed in section 7.

There may be ways to lower the τ_{1c} threshold. They are possibly related to a better choice of the retrieval algorithm and the retrieval size parameter, and to statistical processing of the retrievals. These options are currently being explored.

5. Angular Trends

a. Methodology of tests

Dependence of aerosol retrievals upon sun-view-scattering-reflection geometry serves as yet another test of retrieval performance, since a retrieved parameter should not depend upon any of these

geometrical factors. Ignatov and Stowe (2000), who first described these types of checks, emphasized that they should be applied to space-time boxes with maximally uniform aerosols. The authors also stressed that the usefulness of the tests, which are statistical in their nature, obviously increases with sample size, but only applied them to one orbit of TRMM data, as a preliminary test of the VIRS aerosol retrievals. The four multi-day datasets used in the present study are much better suited for these tests. The desired sampling uniformity was intentionally achieved by carefully choosing the latitudinal belt of 5-25°S, which is known to be generally covered with the fewest and most uniform aerosols around the world (Husar et al. 1997). In section 6, spatial uniformity of the aerosol is checked.

Yet another major development of this study is that self-consistency of the AVHRR retrievals is checked with modified/improved versions of the checks introduced by Ignatov and Stowe (2000). Establishing appropriate PDFs of the derived parameters allowed introducing physically meaningful and mathematically justified definitions for the mean and standard deviation. As a result, the uncertainties of the ensemble mean τ and α can be accurately estimated.

Figs.9-12 show angle trends (view and solar zenith, scattering, and glint angles, respectively) of two aerosol statistics: the mean, with its standard error of estimate, and the minimum. (Maximum τ have also been evaluated, but are not shown here because they require a substantially different scale on the y-axis, which would make the small trends in the mean and minimum difficult to visualize. Using a different right y-axis, and adding one more graph of the maximum, was also tested, but turned out to be impractical. Additionally, despite the rigorous cloud screening in the data, and the QC checks, the maximum τ may be still affected by residual cloud contamination, and therefore difficult to interpret). Mean and its standard error were calculated from data which passed all quality control checks QC1-7; for determination of the minimum, four of the seven QC tests were skipped (QC2-3,6-7). This is done to keep negative τ in the analysis, which are indicative of problems with retrievals. For the Angstrom exponent, the maximum is determined, and the statistics are analyzed for $\tau_1, \tau_2 > 0.05$, to remove noisy

values at low τ which can drastically influence the α_{\min} & α_{\max} values.

For τ_1 and τ_2 (left and center panels in all figures, respectively), the mean is calculated geometrically (τ_g ; as explained in section 2); for α (right panel), it is done arithmetically (α_a). The standard error of the mean is calculated as $\tau_g \times \varepsilon_{\tau_g}$ (upper) and $\tau_g / \varepsilon_{\tau_g}$ (lower) for τ , and as $(\alpha_a + \varepsilon_{\alpha_a}, \alpha_a - \varepsilon_{\alpha_a})$ for α . For N *independent* measurements, values of ε_{τ_g} and ε_{α_a} are calculated as $\varepsilon_{\tau_g} \approx 10^{3 \times \log \mu / \sqrt{N}}$; $\varepsilon_{\alpha_a} \approx 3 \times \sigma_{\alpha} / \sqrt{N}$. Not all measurements in the four datasets can be considered independent, though. Estimates show that on average, one (AEROS) retrieval is obtained within a $\sim(10^2 \text{ km})^2$ box. The spatial statistical structure of atmospheric aerosols is not known at this time. In its place, it is assumed that aerosols vary like other atmospheric meteorological variables such as temperature and humidity. From meteorological statistics, it is known that the correlation structure of these parameters fully disintegrates at scales of $\sim 10^3$ km or so (the so called synoptic scale). Therefore, for calculation of the error bars, we have reduced the number of observations in each dataset by two orders of magnitude (i.e., $N = N_{\text{obs}} / 100$, assuming one independent observation in a $\sim(10^3 \text{ km})^2$ box), to account for their inter-dependency.

b. Minimum τ

The minimum τ_1 and τ_2 are dependent on several factors, in order of most likely significance: 1) calibration of the sensor; 2) surface reflectance; and 3) molecular scattering and absorption used in the retrieval model. Figs.9-12 show that τ_{\min} are typically within $\sim 0-0.05$, but can be negative (e.g., τ_1 in May'99). The least noticeable angular trends in the minima are observed in May'99 (especially in τ_2), whereas in all other datasets, both $\tau_{1\min}$ and $\tau_{2\min}$ tend to increase by $\Delta\tau \sim 0.01-0.02$ over the full range of any of the four angles. It is not clear at this moment how to attribute the above three factors to the observed dependencies in the minima on angle and dataset. Currently, a detailed sensitivity study is underway to separate out these effects. It is unlikely that calibration could cause angular dependencies within a dataset because the uncertainties in calibration are from one dataset to the next, not within a

given dataset. The angular dependencies in the minima may be due to both incorrect treatment of the surface reflectance or of the multiple scattering and absorption by molecules in the retrieval model. For example, preliminary numerical estimates show that lowering the diffuse component of surface reflectance in channel 1 by $\Delta\rho_1^s = -0.002$ (that is, setting it to 0, since it is currently set at $\rho_1^s = 0.002$), does reduce angular variations by about $\Delta\tau_1 \sim 0.01$, while on average raising the retrieved τ_1 by $\sim 0.02-0.03$. Also, it is conceivable that our incomplete treatment of the bidirectional reflectance of the surface (e.g. using the fixed wind speed of 1 m/s in the retrievals) could cause some of the differences between datasets, as the solar zenith angle is very different between them, due to coming from different seasons and also due to drift in satellite orbital equator crossing time.

c. Mean τ

Angular trends in the mean τ could not only be related to modeling errors in surface reflectance or molecular scattering and absorption, but also to errors related to the aerosol model (phase function) used in the retrieval algorithm. Visual inspection of Figs.9-12 suggests that angular trends are observed in the data. In the majority of cases, however, these are statistically insignificant (i.e., are within the uncertainty intervals, except for the sun angle trends in τ_1 and τ_2 at $\theta_s > 60^\circ$ in May'99, due to numerical errors introduced by the retrieval algorithm itself -- see analyses in section 7 of IS01), and are not persistent from one dataset to another. This lack of notable artifacts in the mean retrievals is encouraging, suggesting that the aerosol microphysical model used in the retrieval is close to the real aerosol in this area. Quantitatively, this statement implies that the phase functions used in the retrievals from the two AVHRR channels are most probably adequate within $\Delta P/P \sim \pm 15\%$, because AODs are stable within $\sim \pm 0.02$ ($\Delta P/P \sim \Delta\tau/\tau \sim 0.02/0.13 \sim \pm 0.15$).

Note however that the data used in this study have been collected over oceanic areas with pristine atmospheres (low aerosol amounts), and therefore are better suited for the analysis and

adjustment of non-aerosol parameters of the retrieval model, and of the quality of the input data. For aerosol-model related analyses, atmospheres with higher aerosol content should be sampled, and validation studies conducted, using ground based sun-photometers. Such studies were performed by Ignatov et al. (1995) using ship sun-photometers, and have recently been applied to NOAA14/AVHRR and TRMM/VIRS retrievals by Zhao and Stowe (2001), using AERONET data (Holben et al. 1998).

d. Angstrom Exponent

Even if AODs in the two channels do not reveal statistically significant angular trends, the Angstrom exponent may do so because it is related to the difference of their logarithms (i.e., the differencing may amplify counter-directed trends), additionally amplified through multiplication by the coefficient $\Lambda \sim 3.63$. Indeed, Figs.9-12 show that angular trends in the Angstrom exponent are more notable than in τ . In particular, all angular trends appear to be statistically significant in Jan'99, and some (particularly with scattering angle) in May'99. Plotting angular trends of the Angstrom exponent may thus offer a more efficient tool for identifying otherwise un-detectable trends in τ .

6. Geographical Trends

In Figs.13-14, the same statistics are shown as in the previous section but as a function of latitude and longitude, respectively. These figures check that 1) the analyzed area is uniform enough to warrant the use of consistency checks described in section 5; and 2) residual geographical trends are consistent with the expected distribution of the retrieved parameters.

Overall, the distribution of aerosols with latitude is more uniform than with longitude, where major crossings of the continent/ocean boundaries take place. Small local maxima occur in both τ_1 and τ_2 around 10-15°S in all datasets. In Feb'98 and Apr'98, statistically significant fluctuations in τ_1 and τ_2 are observed off the African coast, and over the Indian ocean in the longitude range of 0-100°E. In Jan'99

and May'99, somewhat smaller, but still statistically significant fluctuations occur near Indonesia (90-150°E), off the west coast of Africa (30°W-30°E), and off the east and west coast of S.America (30-40°W, and 80-90°W). The Angstrom exponent results show that α is elevated off the west coast of Africa, and off the west coast of S.America by a few tenths, whereas the Indian ocean aerosols tend to have a lower Angstrom exponent.

In general, these tests confirm that the 5-25°S region is sufficiently uniform to satisfy the consistency check requirements, and that the fluctuations seen geographically are occurring where known sources of aerosol exist (cf. Husar et al. 1997).

7. Conclusion

Retrievals of aerosol optical depths from AVHRR channels 1 (0.63 μm) and 2 (0.83 μm), τ_1 and τ_2 , and their resulting Angstrom exponent, α , using an improved 6S radiative transfer model, have been examined empirically for self-consistency and tested to see if physically reasonable. Overall, these analyses have indirectly confirmed the suitability of the more physically complete and versatile 6S radiative transfer code for the future development of aerosol algorithms from AVHRR.

Analysis of the statistical distributions (histograms) of the retrievals has shown that, to a good approximation, τ may be considered as distributed log-normally. This result is in agreement with recent findings from ground-based sun-photometers by O'Neill et al. (2000). The Angstrom exponent, α , was found to be distributed normally, which is shown to be theoretically consistent with log-normality of τ . These results are of fundamental importance for aerosol research, as they may provide insightful guidance to many practically important aerosol applications. One is the appropriate reporting of aerosol statistics. To that end, the finding by O'Neill et al. (2000), that geometrical mean optical depth is a better representation of average aerosol over an ensemble of measurements, has been independently confirmed in this study from the satellite perspective. Another implication of these results is that the calculation of

regression statistics of satellite retrievals against sun-photometers for validation purposes, the basis of which depends upon the data being normally distributed, would be more meaningful if done in a “ $\log \tau_{\text{SAT}}$ vs $\log \tau_{\text{SP}}$ ” space. For the Angstrom exponent, a regular linear scale is most appropriate.

Statistics of the four datasets reveal declining trends in τ of about 0.03-0.04 from Feb’98 through May’99. These trends are largely coherent in the two channels, contributing to a more stable Angstrom exponent, α (except May’99), which, however, appears biased low in all cases. From a review of possible causes, it is concluded that these declining trends are unlikely to be related to the retrieval algorithm. As discussed in the first part of this paper, this study also suggests that this trend (if truly continuous over the four datasets) is most probably related to calibration uncertainties, which are currently being analyzed.

A set of seven quality control checks has been formulated to identify and remove outliers. Particularly useful is the spectral test, based on the coherence of τ_1 and τ_2 . Note that this latter test is only possible when *independent* retrievals from the two AVHRR channels are performed. The suite of checks removes a total of ~0.8-1.2% of the data. However, other retrievals which are less noisy than those removed, and are therefore not identified by the QC tests, probably remain in the data, and may still contribute errors to aerosol analyses.

Physical interpretation of the spectral QC test results allowed the estimation of two useful parameters but only for the first three datasets (Feb’98-Jan’99). (Results for the last dataset of May’99 seem unreliable, due to its anomalous characteristics). The first is an unresolved combination of noise from the two AOD retrievals ($\sigma_{1n}^2 + \sigma_{2n}^2$) $\sim 1 \times 10^{-4}$, related to additive error sources. The second is the inherent (true) RMS variability of the Angstrom exponent within the domain of observations which, for the 5-25°S oceanic region, was found to be $\sigma_{\omega} \sim 0.24 \pm 0.02$.

The intercepts of the scattergrams “ τ_1 vs τ_2 ” after QC tests are always < 0.01 , suggesting that the oceanic reflectance model, Rayleigh optical depth, and calibration in the two channels remain inter-

consistent. However, there is inconsistency as AOD increases. Specifically, the “ τ_1 vs τ_2 ” cluster of retrievals does not lie within the expected domain, bounded by two straight lines corresponding to $\alpha=0$ and $\alpha=2$. Instead, the cluster tends to group around the lower boundary of this domain. This could be the result of overestimating water vapor absorption in the channel 2 retrieval model. More analysis is needed to resolve this unrealistic feature.

Using results of previous theoretical analyses by Ignatov et al. (1998), the variability in the retrieved Angstrom exponent was approximated as $\sigma_a^2 = \sigma_{ao}^2 + \sigma_{ae}^2 / \tau_1^2$. The first term here, σ_{ao} , is the actual “physical” variability in the Angstrom exponent, and the second term, σ_{ae} , is variability due to errors (“noise”). The validity of this parameterization was confirmed with the data, and its parameters were empirically estimated in two independent ways: $\sigma_{ao} \sim 0.22 \pm 0.02$, and $\sigma_{ae} \sim (4.2 \pm 0.2) \times 10^{-2}$. From the ratio of these two components, a signal-to-noise ratio, η , was formed, $\eta = (\sigma_{ao} / \sigma_{ae}) \times \tau_1$. This parameter shows that aerosol information content increases linearly with τ_1 . A cross-over point, $\tau_{1c} \sim (0.18 \pm 0.02)$, was defined, at which $\eta=1$. As τ_1 becomes smaller than τ_{1c} , the estimated Angstrom exponent becomes progressively dominated by “noise” (resulting from radiometric error, and departures of the actual ocean-atmosphere, non-aerosol model, parameters from those assumed in the retrievals) and therefore conveys little useful aerosol information. As τ_1 increases, the aerosol information contained in the estimated α increases, although noise is still present.

The threshold of usefulness of the Angstrom exponent from a two channel sensor is mainly dependent on two physical factors: 1) spectral separation of the channels, Λ , defined by Eq.(1) (for the AVHRR/2, $\Lambda=3.63$), which amplifies all errors and uncertainties in the individual channel retrievals; and 2) errors in individual channel retrievals themselves. The latter depend, to some extent, upon the performance of the retrieval algorithm, and may be potentially lowered by improvements to the aerosol retrievals (e.g. simultaneous solution; cf. Ignatov and Stowe 2000). But the role of the retrieval algorithm should not be overestimated. The above estimate of $\tau_{1c} \sim (0.18 \pm 0.02)$ for the AVHRR/2 is a

realistic estimate of the inherent capabilities of this sensor. More analysis is needed to understand to what extent this threshold can be lowered, e.g., by averaging the AOD retrievals in space and time. The τ_c parameter may also be used to compare the information capabilities of different advanced aerosol sensors such as MODIS, SeaWiFS, MISR. These have been specifically designed to provide superior performance of the individual channels (by their being more carefully chosen, by minimizing the non-aerosol component of the signal, and by using better electronic and optical components). These instruments cover a much wider spectral interval than AVHRR/2 with increased numbers of channels, and therefore are expected to lower the above estimate of τ_{1c} . Aerosol retrievals from AVHRR/3 (added 1.61 μm channel, and all three channels have higher precision) onboard the newest NOAA-KLMN satellites, are also expected to be more accurate.

Establishing τ_{1c} provides a few possible implications on the strategy for development of an improved AVHRR/2 retrieval algorithm. First, below a certain threshold of aerosol content ($\sim\tau_{1c}$) it is unlikely that any valid aerosol particle size information (e.g., the Angstrom exponent) can be derived. As a result, in this domain of (low) aerosol optical depths (in which belong the majority of data considered in this study), one can probably do no better than to run retrievals in each of the two channels, independently, as is done in the present study. As shown, these two pieces of aerosol information can be combined, to 1) remove outliers; and 2) to suppress noise in the individual channel retrievals (by e.g. appropriate weighting of the two products, the ways of which are yet to be determined), thus producing a superior estimate of aerosol optical depth in either channel. The output from this “low-aerosol” algorithm can be smoothly merged with the output from a dependent (simultaneous multiple-channel) algorithm, weighted by the retrieved aerosol optical depth.

Consistency checks, formulated elsewhere, have been modified in this study to take into account the log-normal distribution of τ . This development allowed a measure of uncertainty in the trends of τ with sun-view-scattering-reflection angles to be estimated, which was lacking before. This tool was

applied to all four datasets, to test the retrievals. These quality control and consistency checks are used to evaluate the performance of the present algorithm and to assist with the development of the next generation algorithm. Preliminary results suggest that the retrievals are, to a large extent, self- and inter-consistent, although some artificial trends in time, and with different sun-view-scattering-reflection geometries are present. Some of these are expected to be related to calibration inconsistencies, documented in the first part of this study, and others to retrieval model inadequacies. The May'99 dataset shows anomalous behavior in many different ways. As analyzed in the first part of this study, this is most likely attributed to numerical retrieval errors at high solar zenith angle in this dataset (more than half of its observations are taken at $\theta_s > 60^\circ$). How to identify the causes of these trends, is currently being investigated, and the results will be reported elsewhere.

Acknowledgments. We greatly appreciate Mr. John Sapper's contribution to the development of the AEROBS software on the NOAA/NESDIS mainframe, which was used for this study, and helpful comments from Dr. Norm O'Neill, and anonymous reviewers. We are very thankful to Dr. Lee Dantzler (Manager of the NOAA Ocean Remote Sensing Program, NOAA/NESDIS), and Drs. Bruce Wielicki and Bruce Barkstrom (NASA TRMM/CERES, contract L-90987C), for support and encouragement.

References

Angstrom, A., 1964: The Parameters of Atmospheric Turbidity. *Tellus*, **XVI**, 214-223.

Barker, H.W., B.A.Wielicki, and L.Parker, 1996: A Parameterization for Computing Grid-Averaged Solar Fluxes for Inhomogeneous Marine Boundary Layer Clouds. Part II: Validation Using satellite data. *J.Atmos.Sci.*, **53**, 2304-2316.

Bevington, P.R., and D.K.Robinson, 1992: Data Reduction and error Analysis for the Physical Sciences. WCB McGraw Hill, 2nd Ed., 328 pp.

Cahalan, R.F., D.Silberstein, and J.Snider, 1995: Liquid Water Path and Plane-Parallel Albedo Bias During ASTEX. *J.Atmos.Sci.*, **52**, 3002-3012.

Campbell, J.W., 1995: The Log-Normal Distribution as a Model for Bio-Optical Variability in the Sea. *J.Geophys.Res.*, **100**, C7, 13,237-13,254.

Higurashi, A., and T.Nakajima, 1999: Development of a Two-Channel Aerosol Retrieval Algorithm on a Global Scale Using NOAA/AVHRR. *J. Atmos. Sci.*, **56**, 924-941.

Holben B.N., T.F.Eck, I.Slutsker, D.Tanre, J.P.Buis, A.Setzer, E.Vermote, J.A.Reagan, Y.Kaufman, T.Nakajima, F.Lavenu, I.Jankowiak, and A.Smirnov, 1998: AERONET - A federated instrument network and data archive for aerosol characterization, *Rem. Sens. Environ.*, **66**, 1-16.

Husar, R., J.Prospiero, and L.Stowe, 1997: Characterization of Tropospheric Aerosols over the oceans

with the NOAA AVHRR optical thickness operational product. *J. Geophys. Res.*, **102**, 16,889-16,910.

Ignatov, A., L. Stowe, and R. Singh, 1995: Validation of the NOAA/NESDIS satellite aerosol product over the North Atlantic in 1989. *J. Geophys. Res.*, **100**, 5,123-5,132.

Ignatov, A., and L. Stowe, 2000: Physical Basis, Premises, and Self-Consistency Checks of Aerosol Retrievals from TRMM VIRS. *J. Appl. Meteorol.*, **39**, 2259-2277.

Ignatov, A., and L. Stowe, 2001: Aerosol Retrievals from Individual AVHRR Channels: I. Retrieval Algorithm, and Transition from Dave' to 6S Radiative Transfer Model. *J. Atm. Sci.*, current issue.

Ignatov, A., L. Stowe, and R. Singh, 1998: Sensitivity Study of the Ångström exponent derived from AVHRR over the oceans. *Adv. Space Res.*, **21**, 439-442.

Kaufman, Y., 1993: Aerosol Optical Thickness and Atmospheric path radiance. *J. Geophys Res.*, **98**, 2,677-2,692.

King, M., D.M. Byrne, J.A. Reagan, and B.M. Herman, 1980: Spectral variation of Aerosol Optical Depth at Tucson, Arizona between August 1975 and December 1977. *J. Appl Meteorol.*, **19**, 723-732.

Korotaev, G., S. Sakerin, A. Ignatov, L. Stowe, and P. McClain, 1993: Sun-Photometer Observations of Aerosol Optical Thickness over the North Atlantic from a Soviet Research vessel for validation of Satellite measurements. *J. Atm. Ocean. Techn.*, **10**, 725-735.

McClain, E.P., 1989: Global SST and Cloud Clearing for aerosol optical depth estimates. *Int. J. Remote*

Sens, **10**, 763-769.

Mishchenko, M.I, I.V.Geogdzhayev, B.Cairns, W.B.Rossow, and A.Lacis, 1999: Aerosol Retrievals Over the Oceans by Use of Channels 1 and 2 AVHRR data: Sensitivity Analysis and Preliminary Results. *Appl.Opt.*, **38**, 7325-7341.

Morel, A., and L.Prieur, 1977: Analysis of variations in the ocean color. *Limnol.Oceanogr.*, **22**, 709-722.

O'Neill, N.T., A.Ignatov, B.Holben, and T.Eck, 2000: The Log-Normal Distribution as a reference for Reporting Aerosol Optical Depth Statistics; Empirical Tests Using Multi-Year, Multi-Site AERONET Sun Photometer Data. *Geophys.Res.Lett.*, **27**, 3333-3336.

Ostle, B., and L.Malone, 1988: Statistics in Research, Iowa State University Press/AMES, 664 pp.

Rao, C.R.N., and J.Chen, 1996: Post-launch calibration of the visible and near-infrared channels of the Advanced Very High Resolution radiometer on the NOAA-14 Spacecraft. *Int.J.Remote Sens.*, **17**, 2743-2747.

Sathyendranath, S., and L.Prieur, and A.Morel, 1989: A three-component model of ocean colour and its application to remote sensing of phytoplankton pigments in coastal waters. *Int. J. Remote Sens.*, **10**, 1373-1394.

Stowe, L., H. Jacobowitz, G.Ohring, K.Knapp, and N.Nalli, 2001: The Advanced Very High Resolution radiometer Pathfinder Atmosphere (PATMOS) Climate Data Set: Initial Analyses and Evaluations. *J. Clim.*, submitted.

Tanre, D., Y.J.Kaufman, M.Herman, and S.Matoo, 1997: Remote Sensing of Aerosol Properties over Oceans Using the MODIS/EOS Spectral Radiances. *J. of Geophysical Research*, **102**, 16,971-16,988.

Tratt, D.M., and R.Menzies, 1994: Recent Climatological Trends in Atmospheric Aerosol Backscatter derived from the Jet Propulsion Laboratory multilayer backscatter Profile database. *Appl.Opt.*, **33**, 424-430.

Vermote, E., D.Tanre, J.L.Deuze, M.Herman, and J.J.Morcrette, 1997: Second Simulation of the Satellite Signal in the Solar spectrum, '6S': An Overview. *IEEE TGARS*, **35**, 675-686.

Wagner, R., S.Nemesure, and S.E.Schwartz, 1997, Aerosol Optical Depth over Oceans: High Space- and Time-Resolution Retrieval and Error Budget from Satellite Radiometry. *J. Atm. Oceanic Techn.*, **14**, 577-590.

Zhao, X.P., and L.Stowe, 2001: Validation of NOAA aerosol retrievals using AERONERT. Current Issue.

Figure captions

Fig.1. Empirical histograms (needles centered on $\Delta\tau=2\times 10^{-2}$ bins) and their fit with log-normal PDFs (solid line) of τ_1 (a; left panel), and its decimal logarithm, $\log \tau_1$ (b; right panel) in AVHRR channel 1 for the four datasets (1-4). Data have been screened with QC1-7 tests described in Table 1.

Fig.2. Same as in Fig.1 but for AVHRR channel 2.

Fig.3. Empirical histograms (needles centered on $\Delta\alpha=1\times 10^{-1}$ bins) and their fit with log-normal PDFs (solid line) of the Angstrom exponent, α , derived from τ_1 and τ_2 of AVHRR (screened with QC1-7 tests described in Table 1) using Eq.(1) for the four datasets (1-4): (a) $\tau_1, \tau_2 \geq 0.03$; (b) for $\tau_1, \tau_2 \geq 0.10$.

Fig.4. Feb'98 dataset: (1) Scattergrams of " τ_1 vs τ_2 " with the regression line $\tau_1 = b+a\times\tau_2$ (dashed) super-imposed; (2) empirical histograms of regression residuals defined by Eq.(9), $\Delta\tau_1$ (needles centered on $\Delta(\Delta\tau_1)=5\times 10^{-3}$ bins), and their gaussian fit; (3) mean square of the regression residual, $\sigma_{\Delta\tau_1}^2$ versus binned τ_2^2 ; and (4) regression residual, $\Delta\tau_1$, versus τ_2 with $\pm 4\sigma_{\Delta\tau_1}$ curves (dashed) super-imposed: (column a) - original data; (column b) - after iterative QC1 outlier screening.

Fig.5. Same as Fig.4 but for Apr'98 dataset.

Fig.6. Same as Fig.4 but for Jan'99 dataset.

Fig.7. Same as Fig.4 but for May'99 dataset.

Fig.8. Scattergrams of ' α vs τ_1 ' for the four datasets (1-4): (column a) raw data with Mean (solid) $\pm 3\sigma_\alpha$ (dashed) lines super-imposed; (column b) same as (a) but after screening with QC1-7 (see Table 1); (column c) relationship of " σ_α^2 vs binned $1/\tau_1^2$ " with linear fit super-imposed.

Fig.9. Minimum (circle), mean (box) & standard error of mean (whisker), and maximum (circle, for α only) of τ_1 (column a), τ_2 (column b), and α (column c) versus binned view zenith angle (θ_v) for the four datasets (1-4). Horizontal dashed lines are at the mean level of each variable. (Note that the α -statistics in Figs.9-14 have been calculated for $\tau_1, \tau_2 \geq 0.05$ only).

Fig.10. Same as in Fig.9 but versus sun zenith angle (θ_s).

Fig.11. Same as in Fig.9 but versus scattering angle (χ).

Fig.12. Same as in Fig.9 but versus glint angle (γ).

Fig.13. Same as in Fig.9 but versus latitude (ϕ ; negative ϕ in Southern Hemisphere) .

Fig.14. Same as in Fig.9 but versus longitude (λ ; negative λ in Western Hemisphere).

Table 1. Number of Observations used in plotting Histograms (Figs.1-2), and calculating Statistics in Table 2.

QC Test	Attribute	Feb'98	Apr'98	Jan'99	May'99
	N: Original Data	67,092	78,269	101,081	108,286
	$\tau_{1min}/N(\tau_1 \leq 0)/\tau_{1max}$ Original Data	+0.01/0/ 1.00	-0.05/6/ 1.44	0.001/0 /1.25	-0.21/115/ 1.20
	$\tau_{2min}/N(\tau_2 \leq 0)/\tau_{2max}$ Original Data	+0.01/0/ 0.73	+0.02/ 0/1.49	0.002/0/ 1.18	-0.01/7/ 0.89
1	$-\Delta N_{Sp}$: Spectral Test (Section 3)	-503	-386	-780	-811
2	$-\Delta N_{N1}$: ($\tau_1 \leq 0$)	0	0	0	-30
3	$-\Delta N_{N2}$: ($\tau_2 \leq 0$)	0	0	0	0
4	$-\Delta N_{L1}$: ($\log \tau_1 > \log \tau_{g1} + 4 \cdot \log \mu_1$)	-5	-53	-14	-5
5	$-\Delta N_{L2}$: ($\log \tau_2 > \log \tau_{g2} + 4 \cdot \log \mu_2$)	-1	-4	-2	-2
6	$-\Delta N_{S1}$: ($\log \tau_1 < \log \tau_{g1} - 4 \cdot \log \mu_1$)	-37	-87	-254	-354
7	$-\Delta N_{S2}$: ($\log \tau_2 < \log \tau_{g2} - 4 \cdot \log \mu_2$)	-31	-72	-83	-178
	$-\Delta N$: Total Excluded Data (Sum of Previous 7 Lines)	-577 (0.86%)	-602 (0.77%)	-1,133 (1.12%)	-1,380 (1.27%)
	N: Screened Data	66,515	77,667	99,948	106,906
	τ_{1min}/τ_{1max} : Screened Data	0.04/ 0.60	0.04/ 0.56	0.03/ 0.51	0.02/ 0.62
	τ_{2min}/τ_{2max} : Screened Data	0.04/ 0.61	0.04/ 0.56	0.03/ 0.53	0.02/ 0.64

Table 2.
Statistics of Aerosol Optical Depths and Angstrom Exponents.

	Feb'98	Apr'98	Jan'99	May'99
τ_{g1} (Geometric Mean in Ch1)	0.148	0.146	0.130	0.116
μ_1 (Geometric STD in Ch1)	1.417	1.397	1.410	1.594
τ_{g2} (Geometric Mean in Ch2)	0.144	0.140	0.126	0.104
μ_2 (Geometric STD in Ch2)	1.442	1.417	1.434	1.582
<hr/>				
τ_{a1} (Arithmetic Mean in Ch1)	0.157	0.154	0.138	0.128
σ_{τ_1} (Arithmetic STD in Ch1)	0.057	0.053	0.047	0.054
τ_{a2} (Arithmetic Mean in Ch2)	0.154	0.148	0.135	0.114
σ_{τ_2} (Arithmetic STD in Ch1)	0.060	0.052	0.047	0.048
<hr/>				
α_m (Mean Angstrom Exponent) (QC1-7 in Table 1)	0.08	0.15	0.11	0.41
σ_α (STD Angstrom Exponent) (QC1-7 in Table 1)	0.38	0.39	0.42	0.68
α_m (Mean Angstrom Exponent) (QC1-7 in Table 1 & $\tau_1, \tau_1 \geq 0.1$)	0.07	0.11	0.07	0.37
σ_α (STD Angstrom Exponent) (QC1-7 in Table 1 & $\tau_1, \tau_1 \geq 0.1$)	0.33	0.33	0.32	0.40

Table 3. Number of Observations excluded at each iteration step of procedure QC1.

Iteration Number	Feb'98	Apr'98	Jan'99	May'99
0 (Original Data)	67,092	78,269	101,081	108,286
1	-298	-264	-246	-563
2	-175	-100	-305	-128
3	-27	-21	-116	-80
4	-3	-1	49	-26
5	----	----	-43	-12
6	----	----	-16	-2
7	----	----	-5	----
Total excluded	-503 (-0.75%)	-386 (-0.49%)	-780 (-0.77%)	-811 (-0.75%)

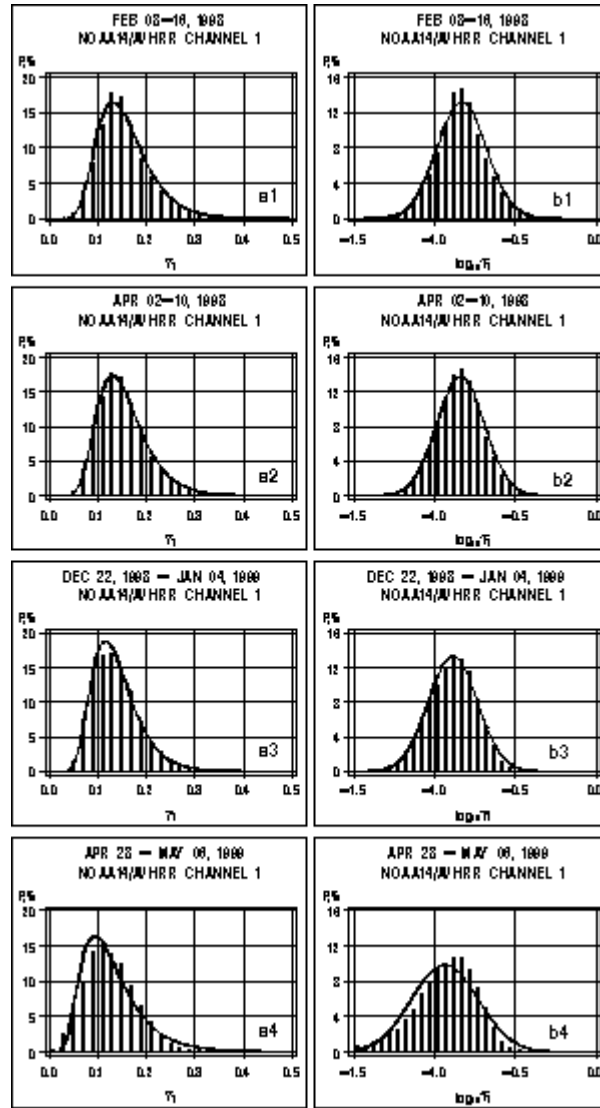


Fig.1. Empirical histograms (needles centered on $\Delta\tau=2\times 10^{-2}$ bins) and their fit with log-normal PDFs (solid line) of τ_1 (a; left panel), and its decimal logarithm, $\log \tau_1$ (b; right panel) in AVHRR channel 1 for the four datasets (1-4). Data have been screened with QC1-7 tests described in Table 1.

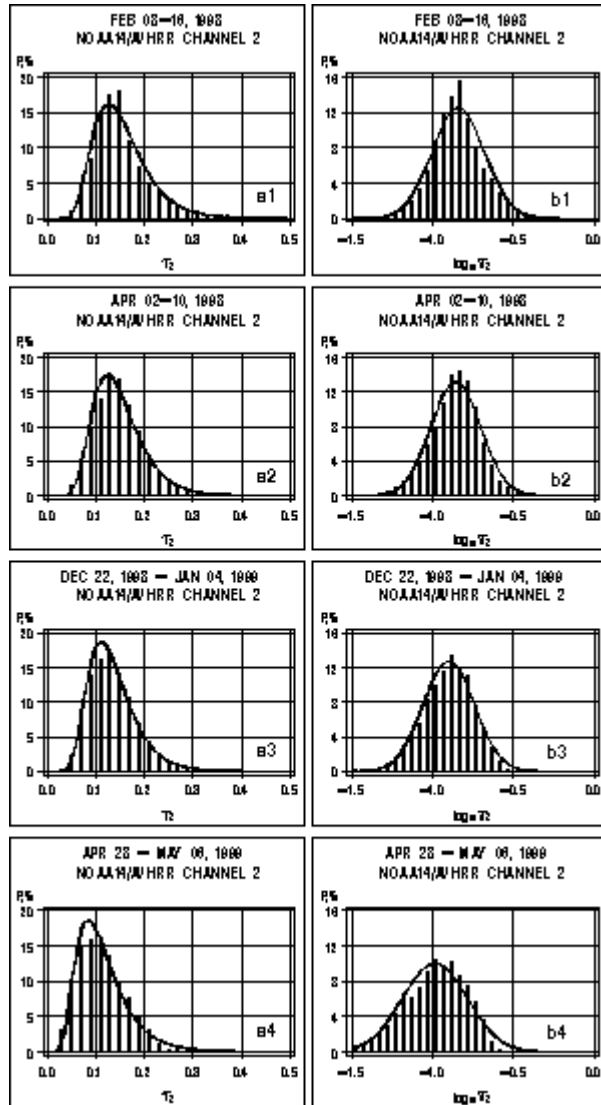


Fig.2. Same as in Fig.1 but for AVHRR channel 2.

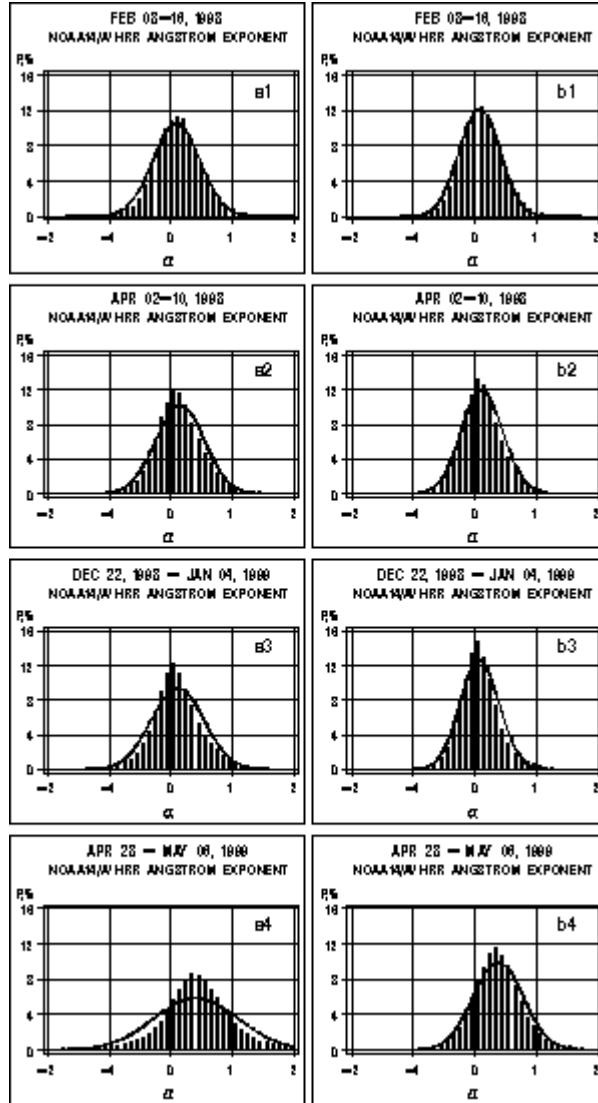


Fig.3. Empirical histograms (needles centered on $\Delta\alpha=1\times 10^{-1}$ bins) and their fit with log-normal PDFs (solid line) of the Angstrom exponent, α , derived from τ_1 and τ_2 of AVHRR (screened with QC1-7 tests described in Table 1) using Eq.(1) for the four datasets (1-4): (a) $\tau_1, \tau_2 \geq 0.03$; (b) for $\tau_1, \tau_2 \geq 0.10$.

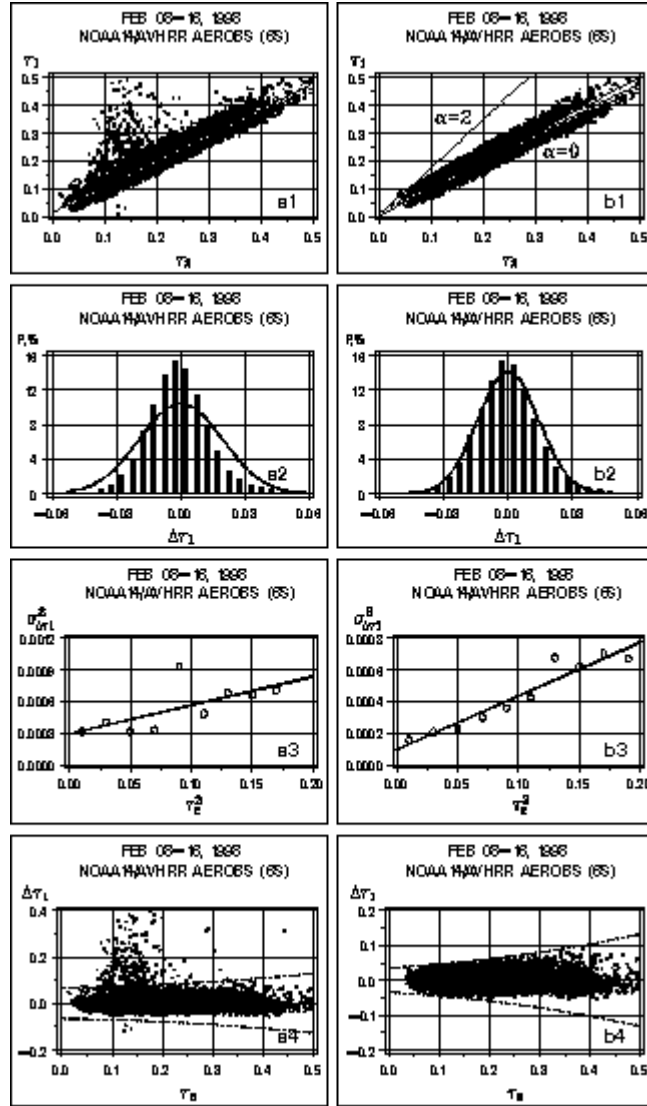


Fig.4. Feb'98 dataset: (1) Scattergrams of " τ_1 vs τ_2 " with the regression line $\tau_1 = b+a \times \tau_2$ (dashed) super-imposed; (2) empirical histograms of regression residuals defined by Eq.(9), $\Delta\tau_1$ (needles centered on $\Delta(\Delta\tau_1)=5 \times 10^{-3}$ bins), and their gaussian fit; (3) mean square of the regression residual, $\sigma_{\Delta\tau_1}^2$ versus binned τ_2^2 ; and (4) regression residual, $\Delta\tau_1$, versus τ_2 with $\pm 4\sigma_{\Delta\tau_1}$ curves (dashed) super-imposed: (column a) - original data; (column b) - after iterative QC1 outlier screening.

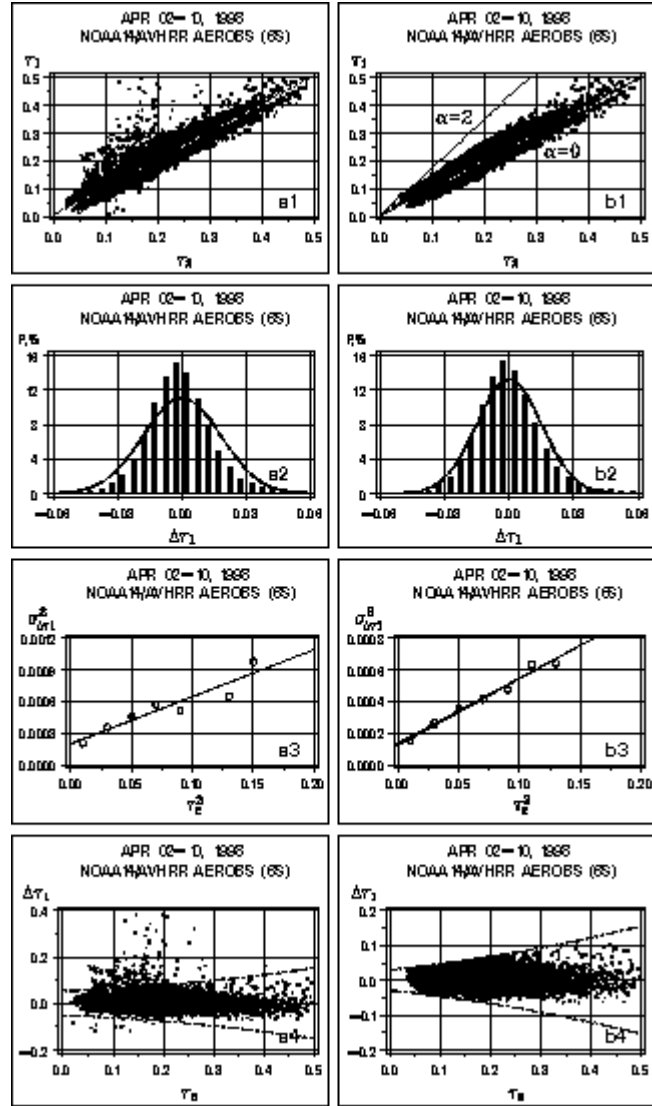


Fig.5. Same as Fig.4 but for Apr'98 dataset.

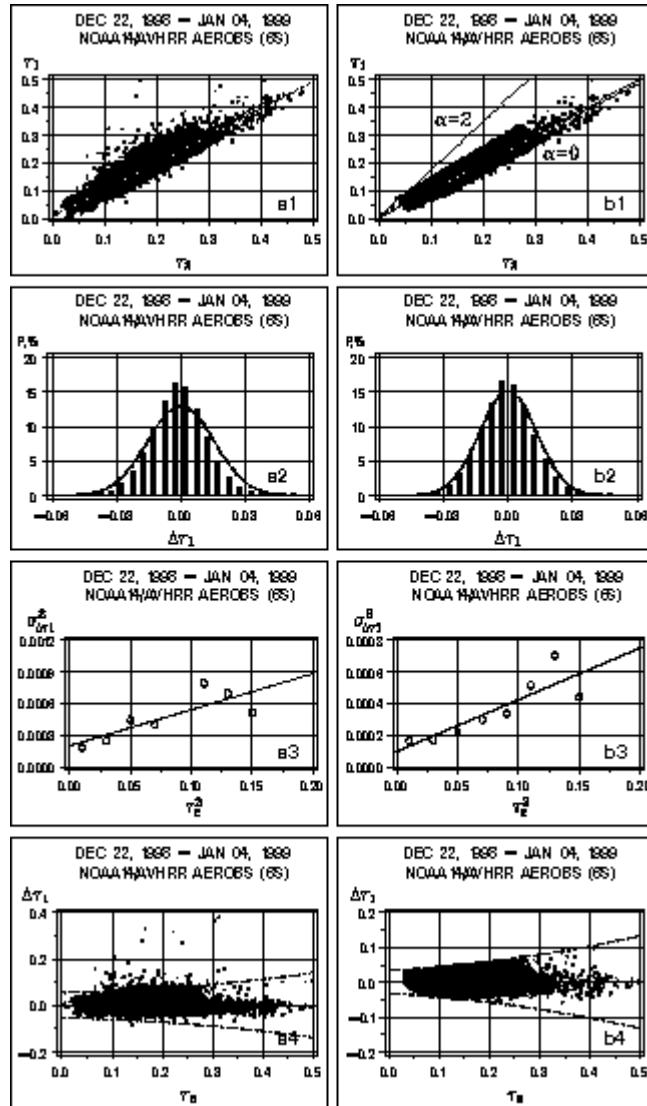


Fig.6. Same as Fig.4 but for Jan'99 dataset.

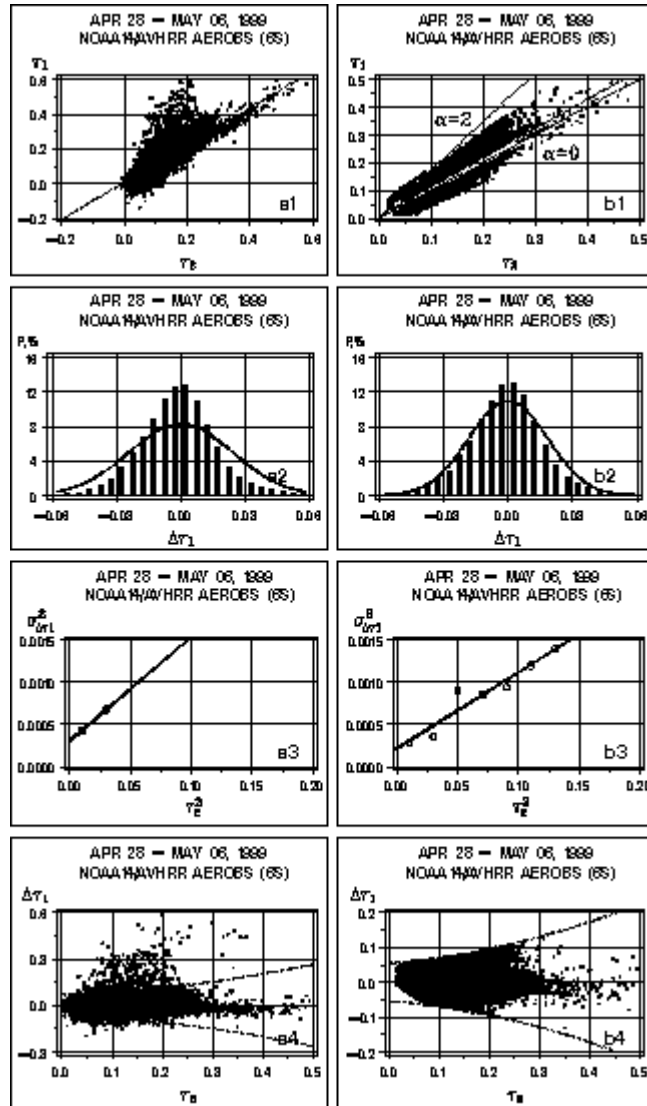


Fig.7. Same as Fig.4 but for May'99 dataset.

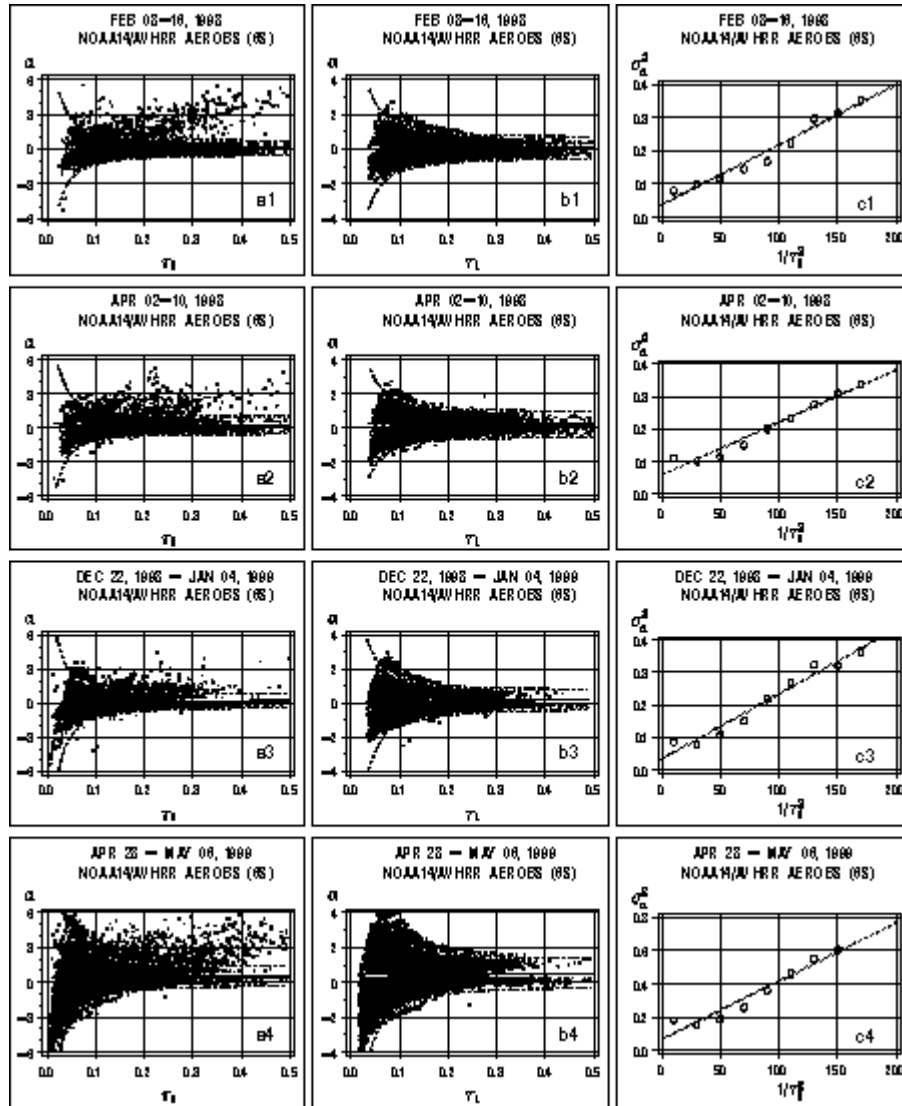


Fig.8. Scattergrams of ‘ α vs τ_1 ’ for the four datasets (1-4): (column a) raw data with Mean (solid) $\pm 3\sigma_\alpha$ (dashed) lines super-imposed; (column b) same as (a) but after screening with QC1-7 (see Table 1); (column c) relationship of “ σ_α^2 vs binned $1/\tau_1^2$ ” with linear fit super-imposed.

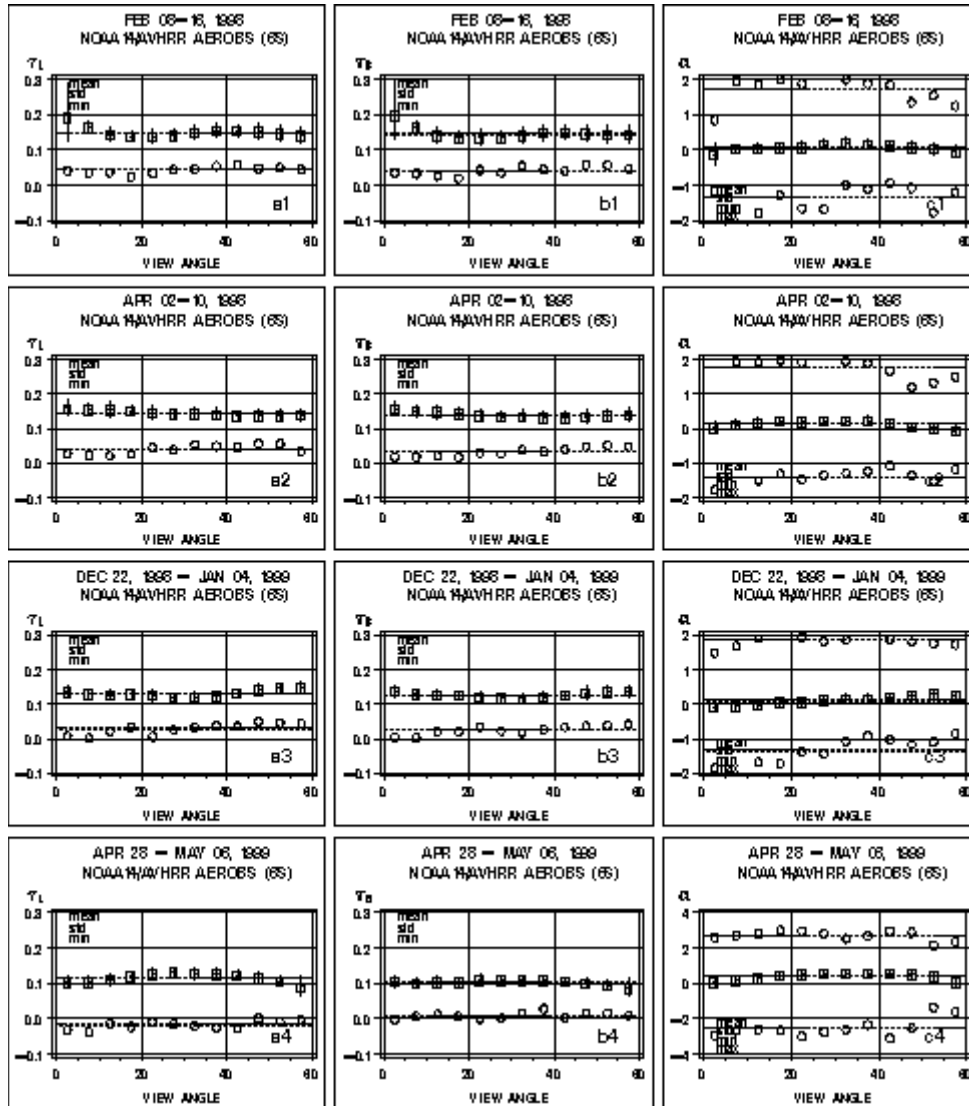


Fig.9. Minimum (circle), mean (box) & standard error of mean (whisker), and maximum (circle, for α only) of τ_1 (column a), τ_2 (column b), and α (column c) versus binned view zenith angle (θ_v) for the four datasets (1-4). Horizontal dashed lines are at the mean level of each variable. (Note that the α -statistics in Figs.9-14 have been calculated for $\tau_1, \tau_2 \geq 0.05$ only).

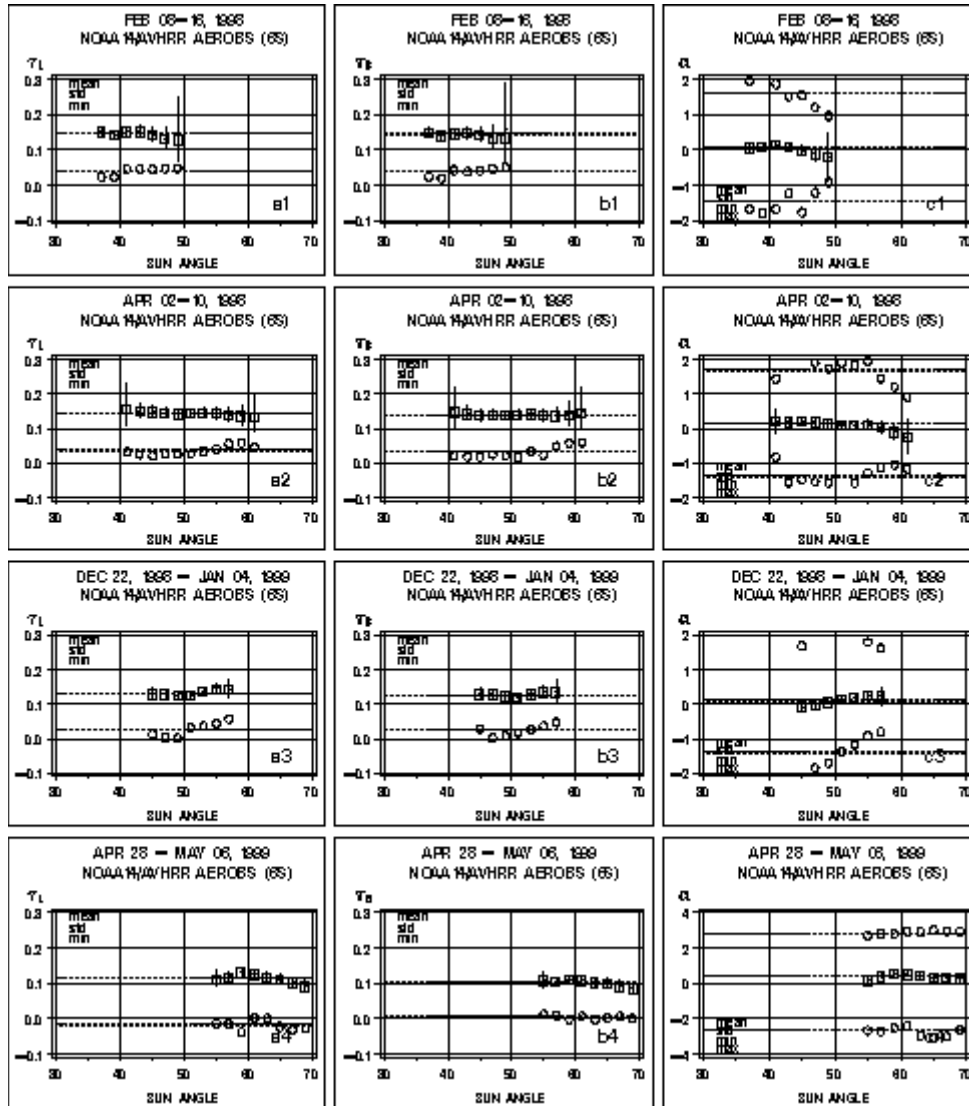


Fig.10. Same as in Fig.9 but versus sun zenith angle (θ_s).

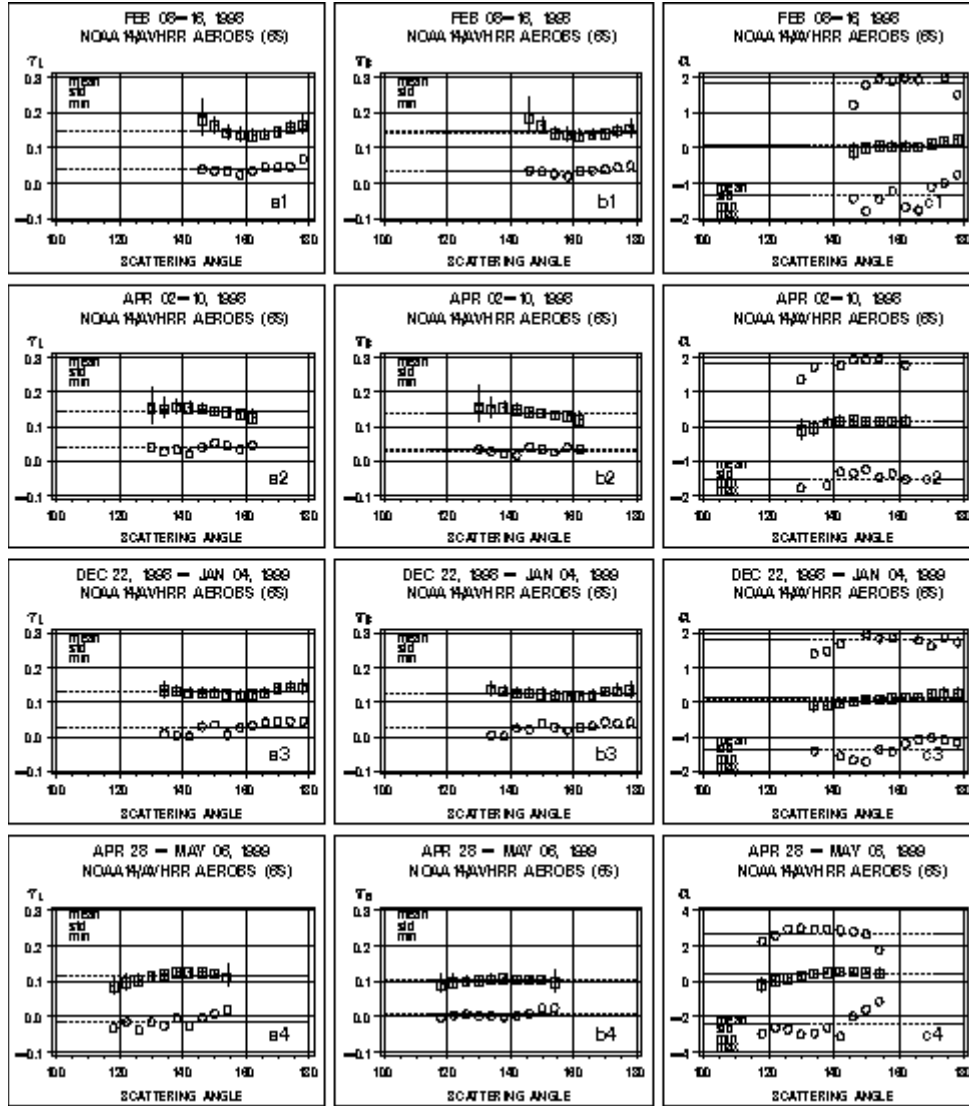


Fig.11. Same as in Fig.9 but versus scattering angle (χ).

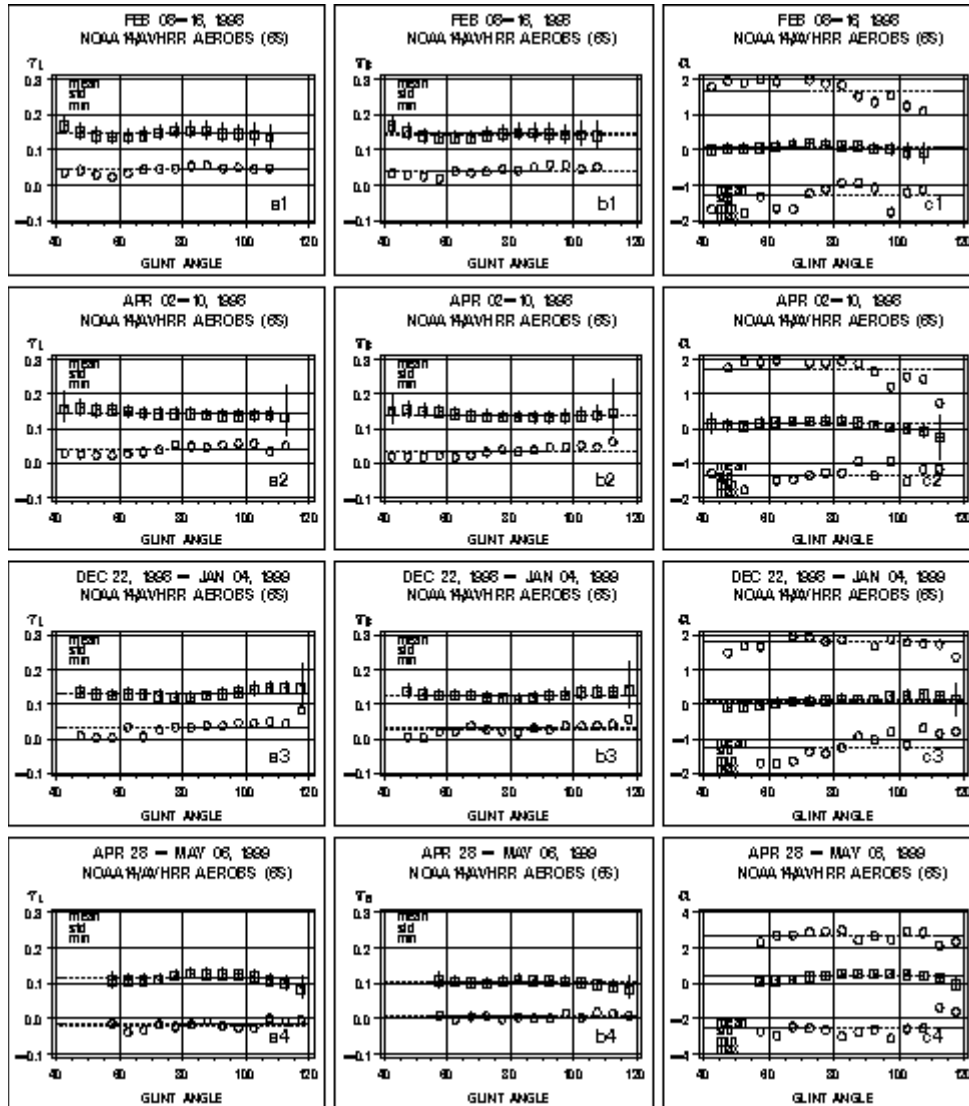


Fig.12. Same as in Fig.9 but versus glint angle (γ).

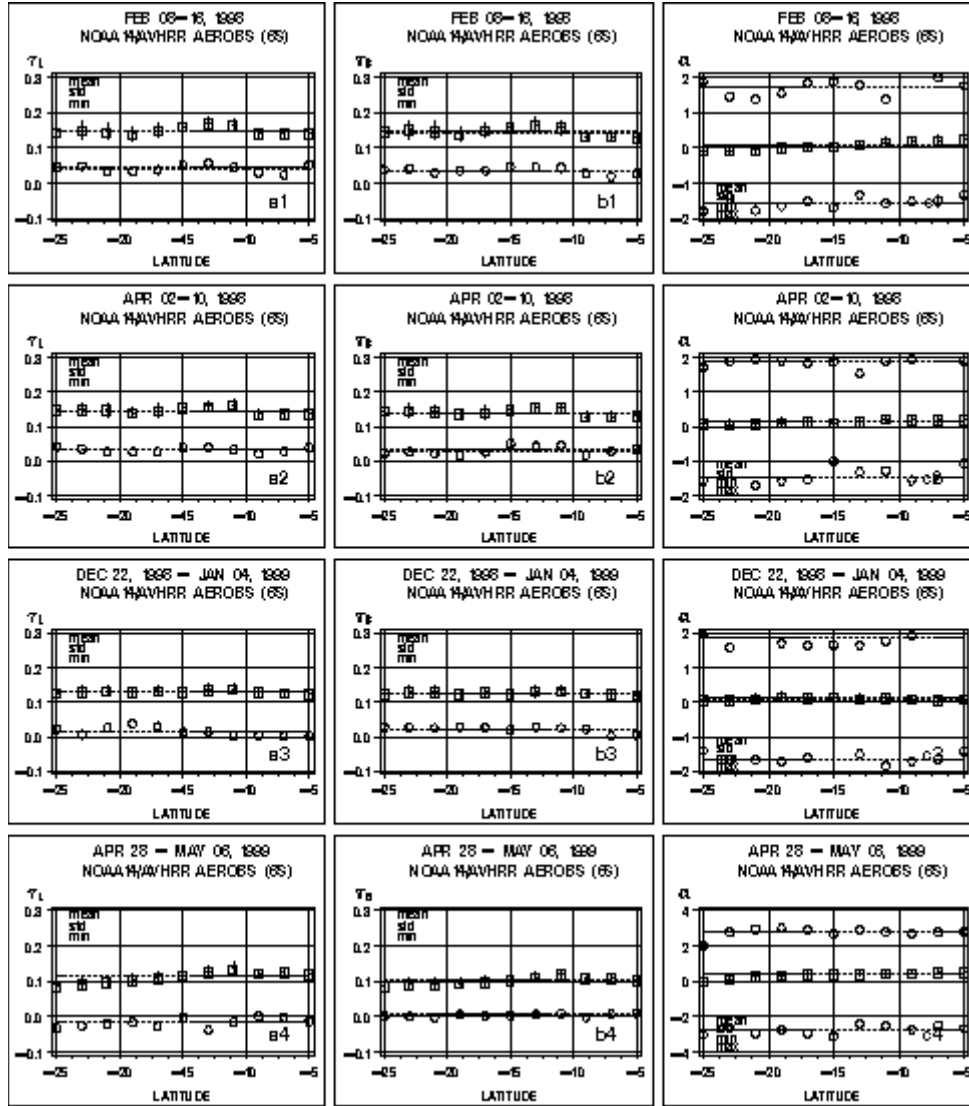


Fig.13. Same as in Fig.9 but versus latitude (ϕ ; negative ϕ in Southern Hemisphere) .

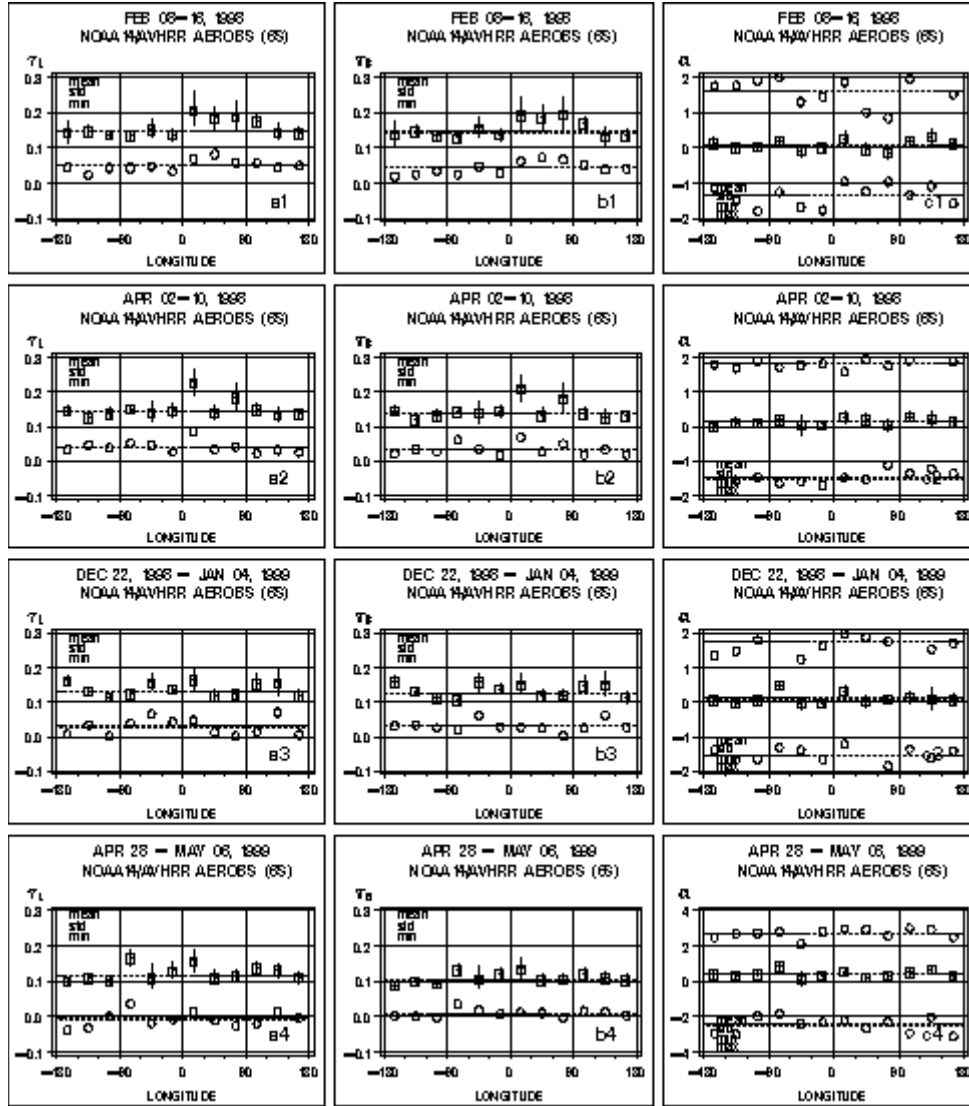


Fig.14. Same as in Fig.9 but versus longitude (λ ; negative λ in Western Hemisphere).